



HAL
open science

Temperature and rheological properties of the mantle beneath the North American craton from an analysis of heat flux and seismic data

F. Lévy, C. Jaupart

► **To cite this version:**

F. Lévy, C. Jaupart. Temperature and rheological properties of the mantle beneath the North American craton from an analysis of heat flux and seismic data. *Journal of Geophysical Research : Solid Earth*, 2011, 116, 10.1029/2010JB007726 . insu-03606504

HAL Id: insu-03606504

<https://insu.hal.science/insu-03606504>

Submitted on 11 Mar 2022

HAL is a multi-disciplinary open access archive for the deposit and dissemination of scientific research documents, whether they are published or not. The documents may come from teaching and research institutions in France or abroad, or from public or private research centers.

L'archive ouverte pluridisciplinaire **HAL**, est destinée au dépôt et à la diffusion de documents scientifiques de niveau recherche, publiés ou non, émanant des établissements d'enseignement et de recherche français ou étrangers, des laboratoires publics ou privés.

Copyright

Temperature and rheological properties of the mantle beneath the North American craton from an analysis of heat flux and seismic data

F. Lévy^{1,2} and C. Jaupart¹

Received 24 May 2010; revised 7 October 2010; accepted 11 November 2010; published 26 January 2011.

[1] We combine heat flux data and seismic velocity models for the North American lithosphere to derive constraints on thermal conditions and deformation mechanisms in the underlying convecting mantle. Local heat flux averages that are not affected by shallow crustal heat production contrasts allow calculation of reliable lithospheric geotherms and uncertainty ranges. For consistency with the seismic data, the mantle potential temperature beneath North America must lie within a 1290°C–1450°C range, close to that for the oceanic mantle sampled at mid-ocean ridges. The heat flux at the base of the lithosphere varies laterally from $11 \pm 3 \text{ mW m}^{-2}$ beneath the $\sim 250 \text{ km}$ thick Archean core of the Superior province to $15 \pm 3 \text{ mW m}^{-2}$ beneath the thinner younger Appalachians province. It is shown that the most likely cause of such rates of heat supply into the North American continent is small-scale convection in an unstable boundary layer beneath the rigid mechanical lithosphere. This allows useful constraints on the mantle rheological properties. We show that the most likely deformation mechanism is dislocation creep in wet mantle rocks. Ranges for the mantle temperature, water content, and rheological parameters could be tightened very significantly once strong constraints are obtained on radiogenic heat production in the lithospheric mantle.

Citation: Lévy, F., and C. Jaupart (2011), Temperature and rheological properties of the mantle beneath the North American craton from an analysis of heat flux and seismic data, *J. Geophys. Res.*, 116, B01408, doi:10.1029/2010JB007726.

1. Introduction

[2] Models for the spatial pattern and velocities of mantle convection have become increasingly complicated over the years and are currently being applied to tectonic events and deformation data with the ultimate ambition of relating the time evolution of geological processes to deep mantle motions [Spasojevic *et al.*, 2009; Forte *et al.*, 2010]. The predictive power of such models relies on the validity of the rheological constitutive equation that is adopted for the mantle and in particular on the dependence of mantle viscosity on temperature. Further, owing to the nonlinear dependence of viscosity on temperature, one additional input must be the average mantle temperature itself. On both counts, current constraints are clearly lacking in precision. A recent review of laboratory data on mantle deformation mechanisms leads to large ranges for the values of the activation energy and volume [Korenaga and Karato, 2008]. Poor constraints on the water content of mantle minerals add further uncertainties. In a similar fashion, current knowledge of the mantle average potential temper-

ature is good to at best $\pm 50 \text{ K}$ [e.g., Katsura *et al.*, 2004; Putirka *et al.*, 2007; Lee *et al.*, 2009]. Thus, the goal of predicting the true mantle viscosity from first principles is still far removed. For this reason, many mantle circulation models have been based not on constitutive deformation laws derived from laboratory measurements but on viscosity values deduced from postglacial rebound studies. Such viscosity determinations, however, rely on the hypothesis of Newtonian behavior, which is not valid for the dislocation creep mechanism. Another limitation is that they provide radial profiles of the horizontally averaged mantle viscosity, and hence say nothing on lateral variations of viscosity due to temperature. From a practical standpoint, one difficulty when dealing with continents is that thermal conditions beneath continental roots may not be identical to those beneath oceans, owing to the insulating character of thick lithosphere and its influence on the large-scale mantle circulation. One constraint on mantle rheology that has been used only rarely is provided by heat flow data, and this subject is pursued here. This constraint is all the more important as it is related to the energy budget of the Earth, which is an essential component of any evolutionary model for our planet.

[3] A scaling law that relates heat flux to rheology and the applied temperature difference has been established for simple convecting systems. This relationship has often been used to predict heat flux and has been at the core of plan-

¹Équipe de Dynamique des Fluides Géologiques, Institut de Physique du Globe de Paris, Paris, France.

²Now at School of Earth and Environment, University of Leeds, Leeds, UK.

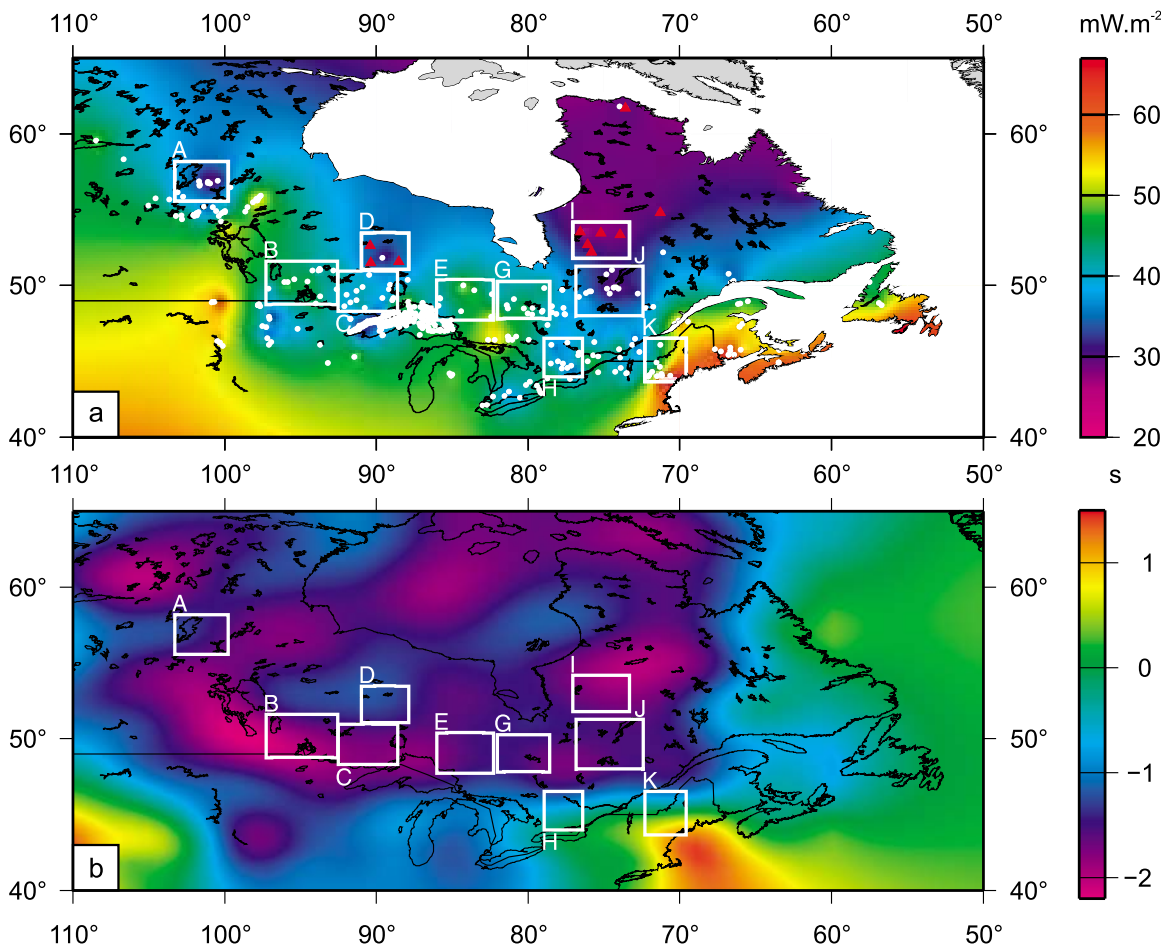


Figure 1. (a) Heat flux map of the Canadian Shield [from Lévy *et al.*, 2010]. (b) Map of S wave travelttime delays for the depth interval 60–300 km, from the NA04 tomographic model of van der Lee and Frederiksen [2005]. The white frames encase the 10 averaging windows used in this study.

etary evolution models over geological time. In the Earth, one can measure heat flow quite easily because of the large thickness of thermal boundary layers. Large-scale heat loss determinations, however, cannot be used to infer mantle physical properties because of inadequate understanding of key aspects of mantle convection, including the generation of large, rigid mobile plates and the initiation of subduction. One consequence is that theoretical models must be “calibrated” by adjusting the theoretical heat flow value for today to the measured one [Korenaga, 2003]. In contrast, small-scale convection at the base of a thick, stagnant lid, such as a continental root, has the advantage of operating over a small temperature range and has been documented in considerable detail [Parsons and McKenzie, 1978; Davaille and Jaupart, 1993; Solomatov, 1995]. Scaling laws for the main characteristics of this form of convection have been obtained for all types of creep laws and checked against numerical calculations and laboratory experiments.

[4] Independently of the large-scale problem of determining the true rheological properties of the Earth’s mantle, thermal conditions at the base of thick continents are of interest in themselves. Heat loss through continents accounts for a significant part of the Earth’s energy budget, and it is important to evaluate the associated physical controls. It

may well be that heat supply at the base of thick continental lithosphere is not achieved by small-scale convection, and this must also be assessed.

[5] In the first part of this paper, we briefly review the characteristics of small-scale convection as well as current constraints on the potential temperature and rheology of the mantle. For the rheology, we compare the strength of constraints brought by heat flow data and viscosity determinations. We seek constraints on thermal conditions in the convecting mantle beneath the Canadian Shield and surrounding provinces, where a large number of heat flux and heat production measurements are now available (Figure 1a). We combine these data with the NA04 tomographic model of van der Lee and Frederiksen [2005] (Figure 1b). This joint analysis allows the resolution of lateral variations of heat flux at the base of the lithosphere and lithospheric thickness. The method and basic objective are similar to those of Lenardic [1997], Doin *et al.* [1997], Jaupart *et al.* [1998], and Lee *et al.* [2005], but we benefit from a much more extensive geophysical data set as well as a much more comprehensive set of rheological parameters due to Korenaga and Karato [2008]. We account for uncertainties in the large number of parameters involved and use robust scaling laws derived

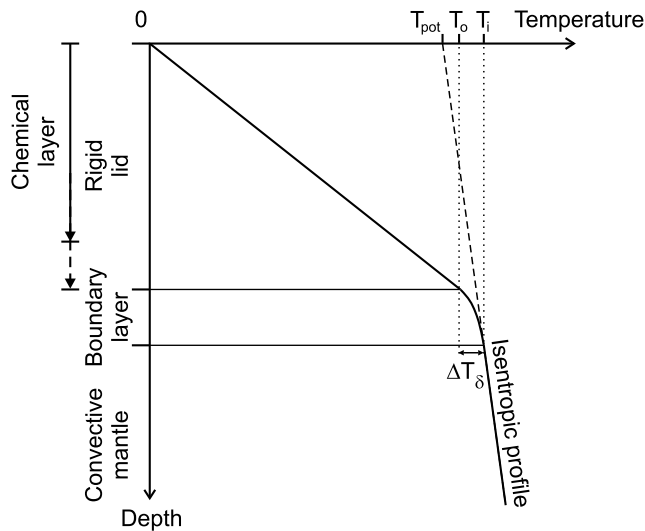


Figure 2. Structure of the continental lithosphere (adapted from Jaupart *et al.* [1998]). The stable and rigid part of the lithosphere, where heat is transported by conduction only, may be made of two sublayers: an upper layer of chemically depleted mantle and a lower layer of undepleted “oceanic-type” mantle that remains stable because of its low temperature and high viscosity. T_{pot} is mantle potential temperature, defined to be the temperature of the mantle isentrope at the Earth’s surface (at a pressure of 10^5 Pa). T_o and T_i are temperatures at the base of the rigid lid and unstable boundary layer, respectively. ΔT_δ is the temperature difference across the unstable basal boundary layer. Depending on the magnitude of ΔT_δ , T_o may be larger or smaller than T_{pot} . T_i , which is equal to $T_o + \Delta T_\delta$, lies along the mantle isentrope. T_i is therefore always larger than the potential temperature.

for both linear and nonlinear creep deformation mechanisms [Solomatov and Moresi, 2000]. We convert geotherms deduced from the heat flow data into vertical profiles of seismic velocity and require them to be consistent with the NA04 tomographic model of *van der Lee and Frederiksen* [2005]. This procedure leads to constraints on the mantle potential temperature, independently of the physical mechanism that supplies heat to the lithosphere. We also determine the thickness of the lithosphere and the heat flux at its base. Comparing the latter with calculated values from rheological equations allows us to determine the most relevant deformation mechanism for the upper mantle. Significant thickness differences are required by the data, so that one deals with convection at different depths in the mantle. Indirectly, this study also provides information on the constitution of the rigid part of the lithosphere (whether it is chemically depleted over its whole thickness or includes a sublayer of viscous undepleted mantle; see Figure 2) [Sleep and Jellinek, 2008].

2. Small-Scale Convection Beneath the Lithosphere

[6] In this paper, we assume that heat is supplied to the lithosphere by small-scale convection, which may coexist

with large-scale circulation with little modification [Parsons and McKenzie, 1978; Doin *et al.*, 1997]. We first discuss one alternative mechanism and then recapitulate some key results on small-scale convection.

2.1. Heating of the Lithosphere by Mantle Plumes

[7] One other mechanism to supply heat to the base of the lithosphere involves mantle plumes coming from a distant interface, presumably the core-mantle boundary. Plume activity is transient by nature, such that it varies in both space and time. Because of the large lithospheric thickness, vagaries of deep heat supply may have no significant thermal impact [Jaupart *et al.*, 1998].

[8] Seismological studies reveal relatively narrow (~ 100 – 200 km) lithospheric anomalies that can be attributed convincingly to mantle plumes. For example, a pronounced low-velocity structure extends through the whole lithospheric mantle beneath the south-central Saskatchewan kimberlite field in Canada [Bank *et al.*, 1998]. Similar anomalies have been found beneath the approximately 200 Ma Monteregean-White Mountain-New England hot spot track in northeastern America or beneath the much older Bushveld intrusion in South Africa [Rondenay *et al.*, 2000; Fouch *et al.*, 2004]. Major plumes are associated with no detectable perturbation to the surface heat flux, owing to efficient lateral heat loss. This is exemplified by the lack of heat flow anomalies in New England and over the approximately 65 Ma Deccan traps region of India [Jaupart *et al.*, 1982; Roy and Rao, 2000]. Major plumes are therefore not appropriate candidates for heat supply to the lithosphere. One may instead appeal to numerous weak plumes that cannot be detected by current geophysical techniques. As shown by *Jurine et al.* [2005], such plumes cannot penetrate chemically depleted lithosphere and pond at its base. How numerous weak plumes can be generated from remote boundary layer instabilities in the Earth’s mantle is far from obvious, however.

[9] A second argument relies on a thermal budget. Considering only stable continents, which occupy an area of about 120×10^6 km², a basal heat flux of 15 mW m⁻² accounts for a total power of about 2 TW. This must be compared to the 2–4 TW estimate for all the known hot spots [Sleep, 1990] over a total oceanic area of about 300×10^6 km². Scaled to the stable continental area, such activity represents less than 2 TW. One would therefore require hidden plumes beneath old continents to be more powerful than all the known hot spots on Earth. Clearly, this hypothesis can be entertained only if small-scale convection can be ruled out convincingly.

2.2. The Characteristics of Small-Scale Convection Beneath a Stagnant Lid

[10] We first consider Newtonian rheology, which is relevant to diffusion creep. Mantle deformation mechanisms involve Arrhenius activation mechanisms, so that the temperature dependence of viscosity takes the following form:

$$\mu = \mu_o \exp\left(\frac{E + PV}{RT}\right) \quad (1)$$

where μ_o is some constant, E is the activation energy, P is pressure, V is the activation volume, and R is the perfect gas

Table 1. Physical Properties of the Upper Mantle

Property	Symbol	Value
Thermal conductivity	k	$3.2 \text{ W m}^{-1} \text{ K}^{-1}$
Thermal expansion coefficient	α	$4 \times 10^{-5} \text{ K}^{-1}$
Thermal diffusivity	κ	$8 \times 10^{-7} \text{ m}^2 \text{ s}^{-1}$
Density	ρ	3350 kg m^{-3}

constant. One may expand this equation for temperatures that are close to that of the well-mixed interior region, T_i :

$$\mu \approx \mu_i \exp \left[-\frac{(E + PV)(T - T_i)}{RT_i^2} \right] \quad (2)$$

where μ_i is the viscosity at the interior temperature T_i . This approximation is valid for the stagnant lid regime because there are only small variations of viscosity and temperature in the actively convecting region. This introduces the rheological temperature scale

$$\Delta T_R = \frac{RT_i^2}{E + PV}. \quad (3)$$

This temperature scale is valid for all Arrhenius activation processes and hence is also relevant for non-Newtonian deformation mechanisms.

[11] With large viscosity variations, convection develops in an unstable boundary layer below a thick stagnant lid, and the appropriate temperature scale is the rheological scale ΔT_R . Viscosity variations in the actively convecting interior are necessarily small, and the heat flux is equal to

$$Q = C_o k \left(\frac{\alpha \rho g}{\kappa \mu_i} \right)^{1/3} \Delta T_\delta^{4/3}, \quad (4)$$

where g is the acceleration of gravity, ρ , k , α , and κ are density, thermal conductivity, coefficient of thermal expansion, and thermal diffusivity, respectively, and C_o is a constant (~ 0.16) [Davaille and Jaupart, 1993; Solomatov, 1995]. Parameter values for the upper mantle are listed in Table 1. In equation (4), ΔT_δ is the temperature difference across the unstable boundary layer and is proportional to ΔT_R [Davaille and Jaupart, 1993; Solomatov and Moresi, 2000],

$$\Delta T_\delta = 2.4 \left(\frac{RT_i^2}{E + PV} \right). \quad (5)$$

For simplicity, we shall refer to these scalings for the heat flux and temperature difference as the rheological scalings.

[12] For nonlinear rheologies, the constitutive relationship between the deviatoric stress and strain rate tensors is written as follows:

$$\dot{\epsilon}_{ij} = \frac{1}{2B} \sigma_2^{n-1} \exp \left(\frac{T - T_i}{\Delta T_R} \right) \sigma_{ij}, \quad (6)$$

where $\dot{\epsilon}$ and σ stand for strain rate and deviatoric stress, respectively; σ_2 is the second invariant of the stress tensor; and B is a constant. Exponent n varies within a large range for dislocation creep in mantle rocks (Table 2). The key feature of such rheologies is that viscosity is not an intrinsic

material property and depends on the applied stress (or on the applied deformation rate):

$$\mu = \frac{\sigma_{ij}}{2\dot{\epsilon}_{ij}} = \frac{B}{\sigma_2^{n-1}} \exp \left(-\frac{T - T_i}{\Delta T_R} \right) = \frac{B^{1/n}}{\dot{\epsilon}_2^{n-1}} \exp \left(-\frac{T - T_i}{n\Delta T_R} \right) \quad (7)$$

where $\dot{\epsilon}_2$ is the second invariant of the strain rate tensor. For $n > 1$, the material exhibits shear-thinning behavior such that the effective viscosity decreases with increasing applied stress. Because of the complex dimension of constant B in equation (7), the convective heat flux expression is more involved than for a Newtonian fluid. We now show that it is still possible to identify the key controls on the strength of convection. Solomatov [1995] and Solomatov and Moresi [2000] have written the convective heat flux due to small-scale convection as follows:

$$Q = \frac{0.31 + 0.22n}{[1.2(n+1)]^{2(n+1)/n+2}} \frac{k(\alpha \rho g)^{n/2}}{[B\kappa \exp \left(\frac{E+PV}{RT_i} \right)]^{1/n+2}} (\Delta T_\delta)^{2(n+1)/n+2}, \quad (8)$$

where the temperature difference driving convection is the following:

$$\Delta T_\delta = 1.2(n+1) \frac{RT_i^2}{E + PV}. \quad (9)$$

We note that Q does not depend on the layer depth and hence that it is determined by local dynamics in the thermal boundary layer independently of the total fluid thickness, as expected for this form of convection. We also note that the heat flux dependence on ΔT_R is stronger than for a Newtonian fluid.

[13] We can rewrite the heat flux equation (equation (8)) in the form of the equation for a Newtonian fluid (i.e., equation (4)), where the temperature difference is specified by equation (9). This defines the effective viscosity for this type of convection,

$$\mu_i = (1.2(n+1))^{6(n+1)/n+2} \left(\frac{0.16}{0.31 + 0.22n} \right)^3 \left[\frac{(B \exp \left(\frac{E+PV}{RT_i} \right))^3}{(\rho g \alpha \Delta T_\delta)^{2(n-1)} \kappa^{n-1}} \right]^{1/n+2}. \quad (10)$$

This equation reduces to the Newtonian form (equation (1)) for $n = 1$. All else being equal, μ_i decreases with increasing values of ΔT_R (or ΔT_δ). This is a direct consequence of shear-thinning behavior: As one increases the temperature difference across the unstable layer, convective vigor increases and hence so does the shear rate. This also implies

Table 2. Flow Law Parameters for Dislocation Creep From Korenaga and Karato, [2008]

	Dislocation	
	Dry	Wet
E (kJ mol ⁻¹)	610 ± 30	523 ± 100
V (cm ³ mol ⁻¹)	13 ± 8	4 ± 3
n	4.94 ± 0.05	3.60 ± 0.24
A	10 ^{6.09±0.11}	10 ^{0.6±0.5}
r	-	1.95 ± 0.05

Table 3. Estimates of Potential Temperature of the Mantle

Temperature	Reference	Method
1315°C	<i>McKenzie et al.</i> [2005]	Depth + heat flux with $k(T)$, $C_p(T)$, $\alpha(T)$
1280°C	<i>McKenzie and Bickle</i> [1988]	Average MORB composition
1315–1475°C	<i>Kinzler and Grove</i> [1992]	MORB composition
1300–1400°C	<i>Lee et al.</i> [2009]	Mineral-melt equilibrium
1400–1450°C	<i>Putirka et al.</i> [2007]	Mineral-melt equilibrium
1257–1347°C	<i>Katsura et al.</i> [2004]	P-T conditions of the Ol-Wa phase change

that the convective heat flux increases more rapidly with increasing ΔT_R than in the Newtonian case. We also note that, for a constant applied temperature difference, μ_i decreases with increasing n because shear-thinning behavior is enhanced. We now show that this effective viscosity corresponds to the stresses involved in small-scale convection.

[14] The scale for convective stresses due to boundary layer instabilities is as follows [*Solomatov and Moresi*, 2000; *Sleep and Jellinek*, 2008]:

$$\sigma \sim \rho_o g \alpha \Delta T_\delta \delta, \quad (11)$$

where δ is the thickness of the unstable boundary layer. This stress scale corresponds to the horizontal pressure difference generated by temperature variations within this thermal boundary layer. Using $Q \sim k \Delta T_\delta / \delta$, we obtain the following:

$$\delta \sim \left(\frac{\rho_o g \alpha \Delta T_\delta}{\kappa \mu_i} \right)^{-1/3}. \quad (12)$$

This allows calculation of the convective stress σ . Substituting this stress into the constitutive equation (equation (7)), we obtain the expression for the effective viscosity μ_i (equation (10)).

3. Thermal Stabilization of Thick Continental Roots

[15] To demonstrate that small-scale convection does account for thermally stable thick lithosphere, we must satisfy two constraints. One is that this thermal equilibrium must be stable to changes of lithosphere thickness and mantle temperature. The other constraint, which forms the bulk of this study, is that this form of convection can supply the required amount of heat. In this section, we review current constraints on mantle properties and temperature and discuss the consequences for small-scale convection in general terms. Detailed quantitative analysis is postponed to sections 5 and 6.

3.1. Properties of the Upper Mantle

3.1.1. Potential Temperature

[16] Values of the oceanic mantle temperature have been derived from the composition of midocean ridge basalts and from an analysis of heat flow and bathymetry data, leading to a total range of 1280°C–1450°C (Table 3). At the scale of the whole mantle, one can use (P, T) conditions for upper mantle phase changes and calculate the temperatures that are implied at the depths of seismic discontinuities. Such temperature estimates can then be continued along isentropes to determine the average mantle potential temperature [*Katsura et al.*, 2004]. Applied to the 410 km discontinuity, this method implies a range of 1257°C–1347°C for the mantle potential

temperature. The various determinations overlap to some extent, but it is difficult to narrow down the range of estimates to less than about 100°C. For typical values of the activation enthalpy for creep, such a range implies an uncertainty of about one order of magnitude for mantle viscosity.

[17] Determinations of the mantle temperature beneath continents are rare and, because they are based on the composition of basaltic melts, usually refer to active regions which may be associated with anomalous mantle. Values at the higher end of the oceanic range have been inferred for the mantle beneath the Basin and Range province and the Colorado Plateau [*Lee et al.*, 2009]. In the case of the Colorado Plateau, there is no evidence for a plume. Using a relationship between basalt composition and source temperature, *Humler and Besse* [2002] have found a trend of increasing oceanic mantle temperature with decreasing distance to the closest continent, which may be due to the insulating effect of continents. The magnitude of this temperature variation is $\sim 50^\circ\text{C}$, which may not be detectable by seismic studies.

3.1.2. Rheological Parameters

[18] The rheological parameters determined from a comprehensive analysis of all available laboratory data by *Korenaga and Karato* [2008] are summarized in Tables 2 and 4. These results confirm the poor constraints on the activation volume and indicate that power law exponents for non-Newtonian deformation regimes span a large range of values.

[19] Diffusion creep leads to a Newtonian flow law. The proportionality constant μ_0 (equation (1)) depends on the grain size and on the water content. For dry mantle,

$$\mu_0 = 10^6 \frac{d^p}{A}, \quad (13)$$

where μ_0 is in Pas, d is the average grain size in microns ($d \sim 10^4 \mu\text{m}$), p is an exponent, and A is a scaling constant. For wet mantle,

$$\mu_0 = 10^6 \frac{d^p}{A C_{OH}^r}, \quad (14)$$

where C_{OH} is water content in ppm H/Si and r is an exponent.

Table 4. Flow Law Parameters for Diffusion Creep [From *Korenaga and Karato*, 2008]

	Diffusion	
	Dry	Wet
E (kJ mol $^{-1}$)	261 \pm 28	387 \pm 53
V (cm 3 mol $^{-1}$)	6 \pm 5	25 \pm 4
A	10 $^{5.25 \pm 0.03}$	10 $^{4.32 \pm 0.38}$
p	2.98 \pm 0.02	2.56 \pm 0.24
r	-	1.93 \pm 0.07

Table 5. Rheological Temperature Scale ΔT_R and Rheological Temperature Difference ΔT_δ for Mantle Rheologies, Using Representative Values From *Korenaga and Karato* [2008]^a

Creep Regime	E (kJ mol ⁻¹)	V (cm ³ mol ⁻¹)	ΔT_R (K)	n	ΔT_δ (K)
Dry diffusion	261	6	81	1	194
Wet diffusion	387	25	45	1	107
Dry dislocation	610	13	35	5	251
Wet dislocation	523	4	44	3.5	237

^a ΔT_R and ΔT_δ are calculated from equations (3) and (9), respectively, with $T_i = 1700$ K at a pressure of 6 GPa.

[20] Dislocation creep is associated with a nonlinear rheology. For dry mantle, constant B in equation (8) is

$$B = \frac{10^{6n}}{A}, \quad (15)$$

and for wet mantle,

$$B = \frac{10^{6n}}{AC_{OH}^r}. \quad (16)$$

[21] Table 5 lists values of the rheological temperature scale ΔT_R and of the temperature difference driving small-scale convection ΔT_δ for representative values of the rheological parameters. One may see that values of ΔT_δ are within a rather small range of about 110–250 K and that dislocation creep is associated with the largest values because of the large rheological exponents.

3.2. Rheological Constraints on the Heat Flux

[22] The ranges of mantle rheological parameters that are consistent with the current experimental data (Tables 2 and 4) do not allow useful predictions of heat supply at the base of the lithosphere. For the sake of example, we have considered a lithospheric thickness of 250 km, a mantle potential temperature of 1350°C and an isentropic gradient of 0.5°C km⁻¹. Calculated heat flux values range from 0.03 to 381 mW m⁻² and therefore span five orders of magnitude.

For wet dislocation creep, which is often the preferred mechanism, heat flux values are still within a large range of 8–381 mW m⁻². This range would have been even larger if we had considered uncertainties on the other constants in the creep law as well as on the water content of the mantle. Adding uncertainties on the lithosphere thickness and mantle potential temperature, the forward prediction of the heat flux is clearly hopeless at present.

[23] This discussion shows a contrario that heat flux data provide useful constraints on the mantle rheological parameters. Another constraint on mantle rheology is provided by the average viscosity values deduced from postglacial rebound studies. Most of such studies rely on the approximation of Newtonian behavior, however, and hence cannot be used to assess results for nonlinear rheologies. In all rigor, one should restrict the discussion to diffusion creep, but dislocation creep is the most probable mechanism for upper mantle deformation [*Korenaga and Karato*, 2008]. Thus, for the sake of simplicity, we use the effective viscosity from equation (10) and compare the relative strengths of constraints on heat flux and viscosity for dislocation creep mechanisms. For an activation volume of 4 cm³ mol⁻¹ (Table 2), an uncertainty of 0.5 log units in the viscosity value leads to a range of 100 kJ mol⁻¹ for the activation energy (Figure 3a). For a conservative range of 10–20 mW m⁻² for the heat flux at the base of the lithosphere, the activation energy must be larger than 570 kJ mol⁻¹ and may be as large as the maximum value derived from the exper-

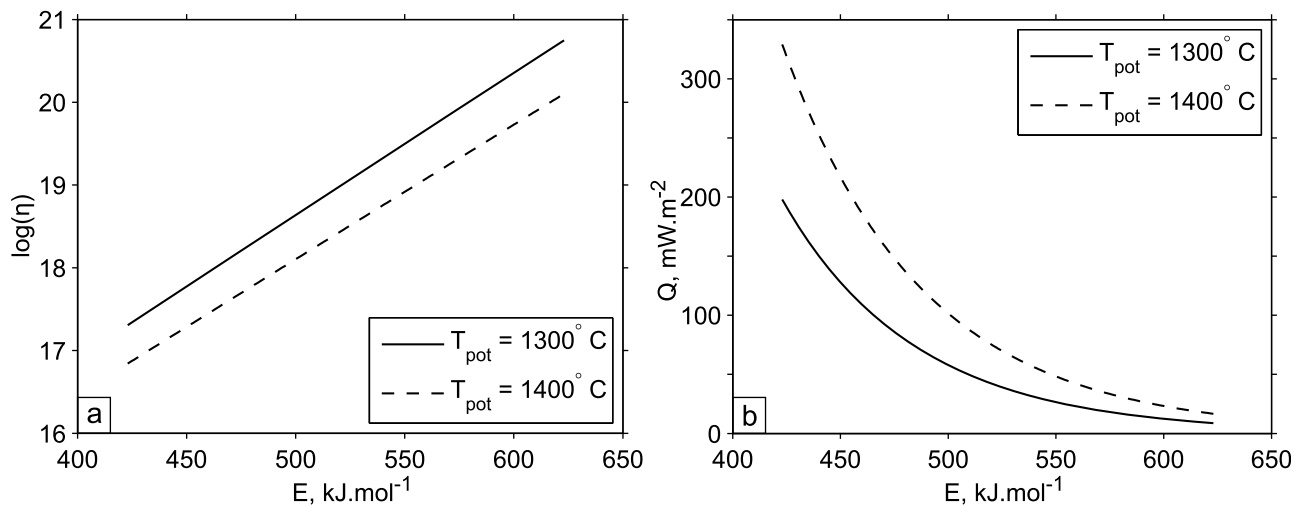


Figure 3. (a) Viscosity and (b) basal rheological heat flux as a function of the activation energy for wet dislocation creep for two mantle potential temperatures. The basal heat flux cannot be constrained from such calculations.

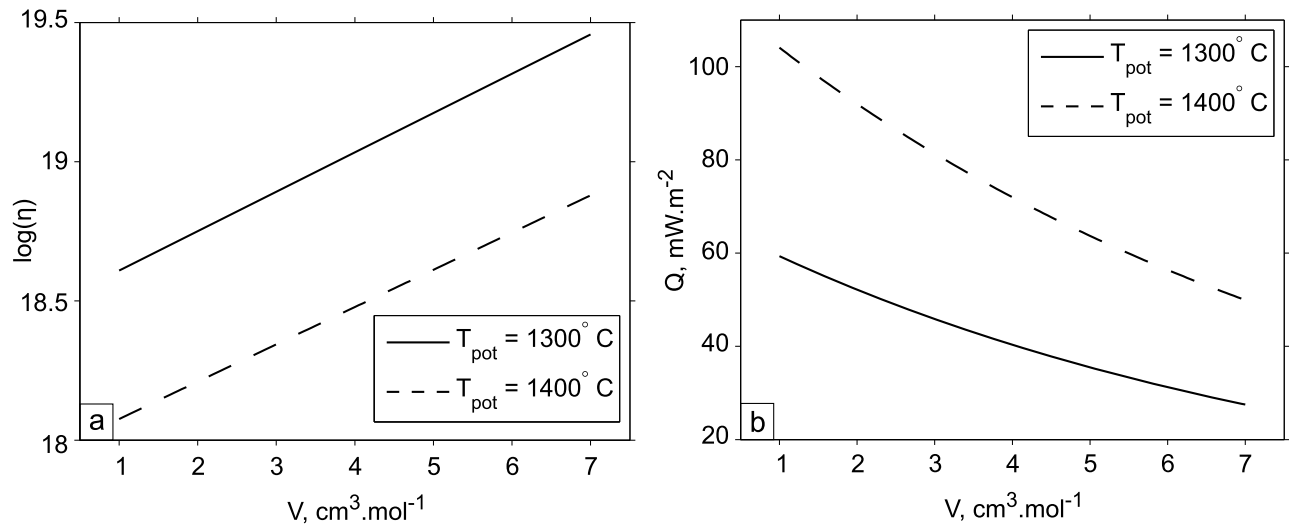


Figure 4. (a) Viscosity and (b) basal rheological heat flux as a function of the activation volume for wet dislocation creep for two mantle potential temperatures. The basal heat flux cannot be constrained from such calculations.

imental data, 630 kJ mol^{-1} (Figure 3b). Constraints on the activation volume are evaluated in Figure 4.

[24] We conclude that heat flow data provide constraints that are as powerful as those of viscosity data. In this paper, we shall also derive constraints on the mantle potential temperature and hence arrive at a self-consistent set of rheological parameters.

3.3. Conditions for a Stable Thermal Equilibrium

[25] Thermal equilibrium in the rigid lithosphere is achieved if the convective heat flux is evacuated by conduction. Denoting by Q the convective heat flux and by T_o the temperature at the base of the rigid lithosphere (Figure 2) and neglecting radiogenic heat production, this balance is such that

$$k \frac{T_o - T_s}{h_o} = Q = k \frac{\Delta T_\delta}{\delta} \quad (17)$$

where h_o denotes the thickness of the mechanical lithosphere and T_s denotes the surface temperature (taken to zero). For an interior mantle temperature T_i , one has

$$T_o + \Delta T_\delta = T_i. \quad (18)$$

Using the scaling laws for Q (equations (4) and (8)), these two equations can be solved for both T_o and h_o . The basal convective heat flux decreases with increasing lithosphere thickness, and so does the conductive heat flux through the lithosphere, as shown by equation (17). The depth dependencies of the two types of heat flux are different and, in some cases, allow two solutions to the heat flux balance. One example is shown in Figure 5. Calculations account for radiogenic heat production and for variations of the well-mixed mantle temperature along an isentrope, such that

$$T_i = T_{\text{pot}} + \gamma z, \quad (19)$$

where $\gamma = 0.5^\circ\text{C km}^{-1}$. In Figure 5, two equilibrium solutions are obtained for thicknesses of about 120 and 380 km,

corresponding to high heat flux through thin lithosphere and low heat flux through thick lithosphere, respectively. Taken at face value, this result is tantalizing, as it suggests that small-scale convection can account for both oceanic and continental lithospheres. However, as pointed out by *Doin et al.* [1997], one must also assess whether the two equilibrium states are stable and how they can be achieved in practice. To this aim, one must consider how the conductive heat flux changes when it is not in equilibrium with the convective one.

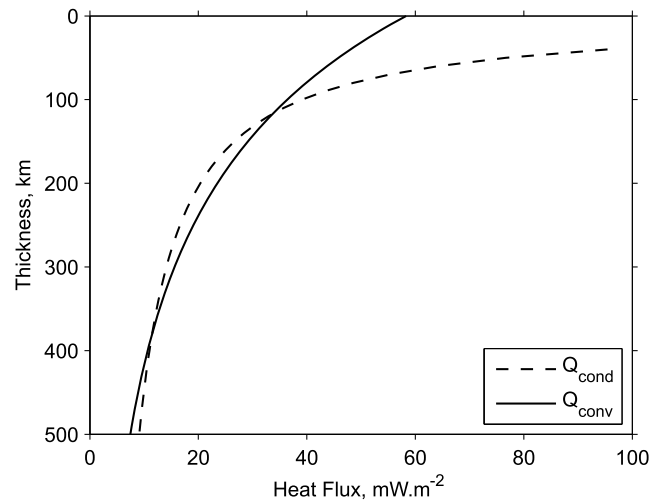


Figure 5. Conductive (Q_{cond}) and convective (Q_{conv}) heat fluxes as a function of lithosphere thickness. The sublithospheric mantle deforms by wet dislocation creep with $C_{OH} = 800 \text{ ppm H/Si}$ and a potential temperature of 1400°C . Rheological parameters are set at the average values of Table 2, except for the activation volume, which is fixed at $15 \text{ cm}^3 \text{ mol}^{-1}$. Calculations include an average crustal radioactivity of $2 \mu\text{W m}^{-3}$. The two heat flux curves intersect at two points which define two equilibrium solutions. As explained in text, only the upper solution is stable.

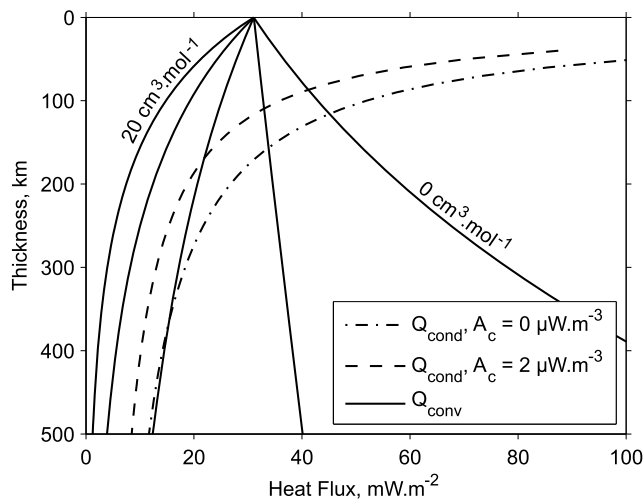


Figure 6. Same as Figure 5 but for different values of the activation volume and two different values of crustal heat production and for a potential temperature of 1300°C . Values of the activation volume V are shown at increments of $5\text{ cm}^3\text{ mol}^{-1}$. There is only one equilibrium solution for $V < 10\text{ cm}^3\text{ mol}^{-1}$, and it is stable. For $5 < V < 10\text{ cm}^3\text{ mol}^{-1}$, this stable solution is achieved for large lithospheric thickness.

[26] If we assume that there is no compositional difference between the lithospheric mantle and convecting mantle below, the lithosphere behaves rigidly because it is cold: This is the “pure” stagnant lid regime. In this case, the lithosphere thickness can change as temperatures evolve. On the one hand, if the convective heat flux is larger than the conductive one, the lithosphere heats up and thins, implying that the conductive heat flux increases. On the other hand, if the convective heat flux is less than the conductive one, the lithosphere cools down and hence thickens, so that the conductive heat flux decreases. This shows how lithosphere thickness and heat flux can adjust themselves to achieve thermal equilibrium. As shown by Figure 5, however, the thickness changes in two different ways in the vicinity of the two equilibrium states. The upper equilibrium state may be attained from both a thin or a thick lithosphere. In contrast, the lower equilibrium state can be achieved only if the lithosphere is created with precisely the right thickness. Starting from lithosphere that is either too thick or too thin, the lithosphere cannot tend toward this equilibrium state and it is not a stable one. This negative conclusion may not be valid, however, because it relies on specific values for the rheological parameters. Furthermore, it does not account for the intrinsic density and viscosity contrast that exists between the chemical lithosphere and the underlying convective mantle.

[27] Figure 6 shows how the two types of heat fluxes vary with lithosphere thickness for various values of the activation volume and for wet dislocation creep parameters. These results illustrate clearly the importance of the activation volume. For small values of the activation volume, there is only one equilibrium thermal state, and it is stable. No equilibrium solution can be found for activation volumes that are larger than $12\text{ cm}^3\text{ mol}^{-1}$. It is interesting to note that equilibrium solutions with acceptable values of litho-

spheric thickness are found for values of V within a $0\text{--}8\text{ cm}^3\text{ mol}^{-1}$ range, which is precisely the range indicated by *Korenaga and Karato* [2008].

[28] Solutions to the thermal equilibrium equation are also somewhat sensitive to the amount of crustal heat production (Figure 6). Interestingly, the equilibrium lithosphere thickness, when it exists, increases as the crustal heat production decreases. The effect is greatly enhanced for values of the activation volume around $10\text{ cm}^3\text{ mol}^{-1}$. This may offer an explanation for lithosphere that is thicker beneath Archean crust than beneath younger enriched crust.

[29] The impact of the mantle potential temperature is assessed in Figure 7. Values of the conductive heat flux are weakly affected by variations of T_{pot} within the small range that is allowed. In contrast, values of the convective heat flux decrease markedly with decreasing T_{pot} . One should note that at least for the set of rheological parameters that has been used in Figure 7, there are stable solutions for thick lithosphere within a rather tight range of mantle potential temperatures.

[30] Finally, we evaluate the same thermal equilibrium diagram for diffusion creep, which involves larger activation volumes. Grain sizes in the upper mantle can be determined from data on xenoliths and massif peridotite samples and from seismic wave attenuation. According to *Jackson et al.* [2002], the range allowed by seismic data is $0.1\text{--}10\text{ mm}$, but most authors consider the $1\text{--}10\text{ mm}$ range to be more realistic. We first fix the grain size to a value of 1 cm as in the work by *Korenaga and Karato* [2008]. For dry diffusion (Figure 8), there are solutions for the small values of the activation volume indicated by the laboratory data (Table 4), but they correspond to unrealistically large lid thicknesses. For wet diffusion, there is no solution for the activation volume indicated by the laboratory data (Table 4). It takes grain sizes of 0.1 mm or less to obtain realistic solutions with wet diffusion (Figure 9). Even for such extreme grain sizes, dry diffusion creep does not work (Figure 10). In the

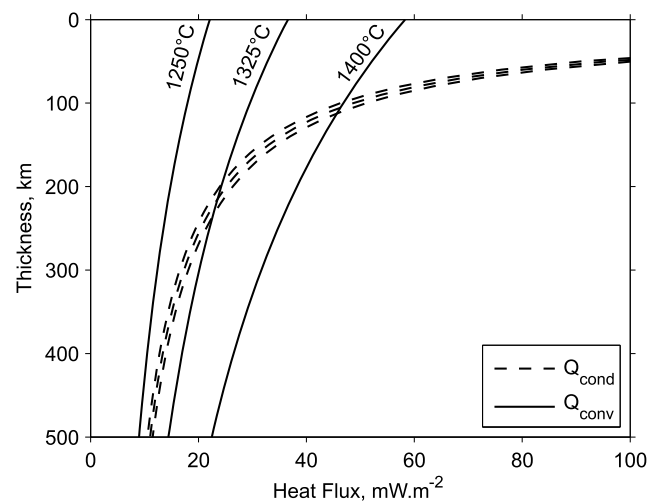


Figure 7. Same as Figure 5 but for three different mantle potential temperatures. The activation volume is set at $10\text{ cm}^3\text{ mol}^{-1}$, and crustal heat production is set at 0.5 μW m^{-3} . There is one stable equilibrium solution. For $T_{\text{pot}} = 1325^{\circ}\text{C}$, this solution corresponds to a lithospheric thickness of about 220 km .

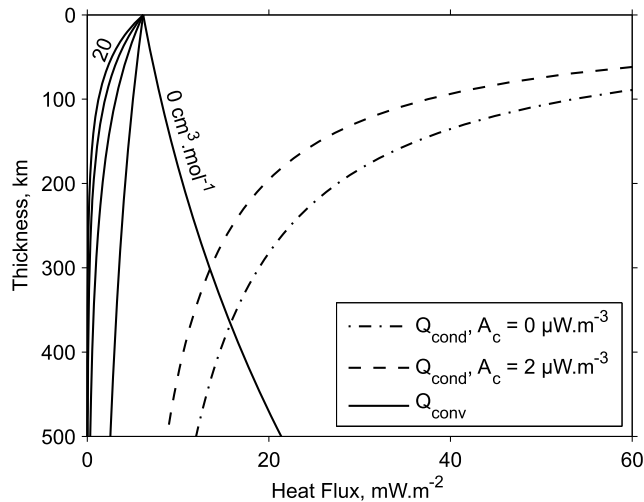


Figure 8. Same as Figure 5 but for a sublithospheric mantle that deforms by dry diffusion creep, with a potential temperature of 1350°C and a grain size of 1 cm. Rheological parameters are set at the average values of Table 4. There are solutions for the small values of the activation volume indicated by the laboratory data, but they correspond to unrealistically large lid thicknesses.

following, we explore the other parameters for the diffusion creep regime.

[31] One final point is that parts of the lithosphere are in fact stabilized by chemical depletion, such that they are both intrinsically buoyant and more viscous than the convective mantle. Such lithosphere cannot be thinned because of an imbalance between the convective and conductive heat fluxes. Thinning may be achieved by mechanical erosion, as envisaged by *Sleep* [2003a], but this is an entirely different mechanism which involves other physical controls. For such lithosphere, as noted by *Sleep and Jellinek* [2008], the temperature difference in the convective basal boundary layer may be smaller than the rheological value (equation

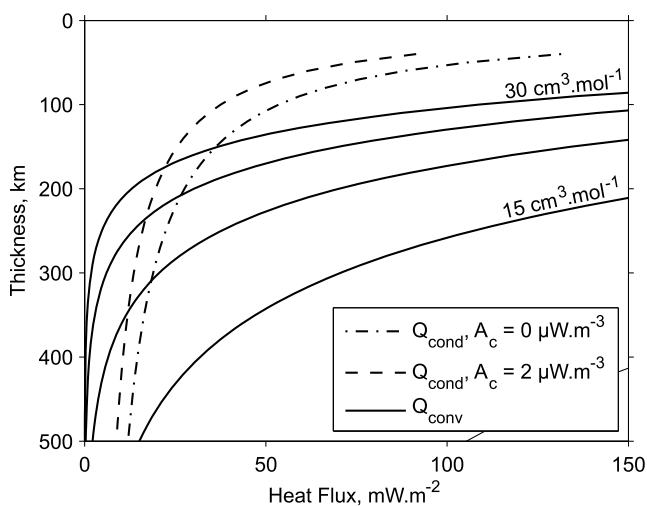


Figure 9. Same as Figure 8 but for wet diffusion creep with $C_{OH} = 800$ ppm H/Si and a grain size of 0.1 mm. Wet diffusion creep works only for grain sizes of 0.1 mm or less that are not considered realistic.

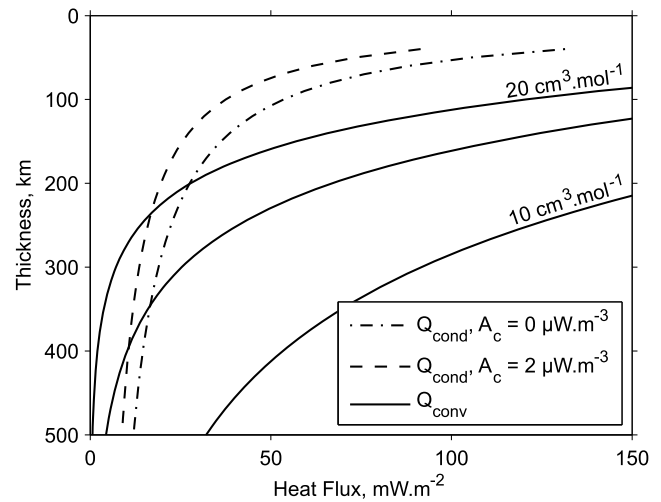


Figure 10. Same as Figure 8 but for a grain size of 0.1 mm. There is no solution for the small activation volumes indicated by laboratory data.

(9)). Thus, there is one additional degree of freedom in the controls on the convective heat flux.

[32] For chemically depleted lithosphere, we suppose that there is initially no thermal equilibrium. This depends, of course, on where the thickness lies with respect to the upper and lower equilibrium states. We briefly discuss the three possible situations that may arise in descending order. Suppose first that the lithosphere is thinner than the upper equilibrium solution. Thickening is possible, and equilibrium is achieved with a rigid lid that includes both the chemical lid and a viscous sublayer. In this case, ΔT_{δ} , the temperature difference across the convective boundary layer, must be equal to the rheological value (equation (9)). Next, we imagine that the chemical lithosphere is thicker than the upper equilibrium state, but thinner than the lower equilibrium one. With a compositional contrast, thinning cannot be achieved by a purely thermal process and the lithosphere would heat up, which would lead to a value of ΔT_{δ} that is smaller than the rheological values as in the work by *Sleep and Jellinek* [2008]. Finally, if the chemical lithosphere is initially thicker than the lower equilibrium state, it would thicken indefinitely because the convective heat flux can never balance the conductive one. The important conclusion is that establishing the conditions for a thermally stable lithosphere has implications for the behavior of continental lithosphere through time as well as for the initial conditions (i.e., thickness) upon its formation through a depletion event.

[33] The above calculations show that one can achieve stable thermal equilibrium with thick lithosphere that is heated from below by small-scale convection. In section 4 we explore the range of rheological parameters that allow such an equilibrium with lithosphere characteristics that are consistent with heat flux and seismic data.

4. Data and Methods

4.1. Heat Flux and Seismic Data

[34] A lengthy and detailed discussion of both heat flow and seismic data is given by *Lévy et al.* [2010], and the most

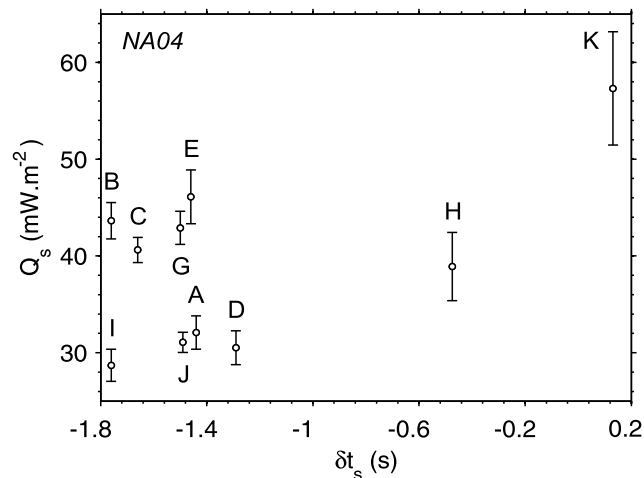


Figure 11. Mean surface heat flux versus mean S wave vertical traveltime delay from the NA04 tomographic model for the 10 windows of Figure 1.

salient points are listed in Appendix A. We combine surface heat flux and heat production data with traveltime delays from the NA04 tomographic model of *van der Lee and Frederiksen* [2005]. Heat flux data in North America are reliable for two reasons. One is that many determinations rely on measurements in two deep neighboring boreholes or more, which allows a better assessment of the measurement reliability and the detection of shallow perturbations. The other reason is that the correction for past climatic changes that must be applied to the data has been carefully calibrated using very deep boreholes distributed throughout the continent. Available measurements now offer a relatively dense coverage of the Canadian Shield and adjacent provinces (Figure 1). With this data set, one may avoid local heat flux anomalies due to shallow heat production contrasts that are not representative of the deep lithospheric thermal structure.

[35] For comparison with seismic data and studies of lithospheric thermal structure, one must continue downward vertical temperature profiles to great depths. The procedure is only reliable if short wavelength anomalies are avoided. This requires determination of average heat flux and heat production values that are representative of the bulk crustal heat production. *Lévy et al.* [2010] have discussed these issues in great detail and have determined averages over 10 geographical windows with the appropriate characteristics. These windows, with typical dimensions of 250×250 km, are distributed over the whole Canadian Shield (Figure 1) and contain enough measurements to ensure the smoothing of small-scale crustal heterogeneities.

[36] We have integrated vertical velocity profiles from the NA04 tomographic model [*van der Lee and Frederiksen*, 2005] to calculate travel times through the lithosphere and have averaged them over the same geographical windows as the heat flux data. The true spatial resolution of the NA04 model is around 200 km, which is smaller than the smallest window size. Traveltime delays are calculated with respect to a specific reference model, and we consider not absolute values but differences between windows. Traveltime calculations and their uncertainties are reviewed in Appendix A.

[37] Recent seismological investigations of lithospheric layering in North America are discussed in Appendix B. In this study, we shall focus on windows I and K, which are associated with the extreme values of average heat flux and traveltime delays (Figure 11). The other windows naturally lead to lithospheric parameters that are within the range defined by these two windows. Window I is located in the Archean Superior Province, east of James Bay. It is characterized by a low surface heat flux (28.7 ± 1.6 mW m⁻²) and a large negative delay (-1.76 s), which suggests a cold underlying lithospheric root. Window K is located in the Appalachians, a relatively narrow Paleozoic belt at the edge of the Canadian Shield. It has a high average surface heat flux (57.3 ± 5.8 mW m⁻²) and a slightly positive traveltime delay ($+0.13$ s). The upper crust of the Appalachians is characterized by an abundance of granites and metasediments with large U, Th, and K contents, which accounts for the elevated heat flux [*Jaupart et al.*, 1982; *Pinet et al.*, 1991]. This province was subjected to several recent perturbations, including the Devonian Acadian Orogeny and culminating in the intrusion of the highly enriched granite bodies of the White Mountains magma series. For our present purposes, we must assess whether the lithosphere of this province is in thermal steady state. Away from enriched granitic bodies, the average heat flux is normal for a province of this age [*Jaupart et al.*, 1982]. Indeed, there is no change of heat flux when going from the Appalachians to the adjacent older Grenville province of Proterozoic age. Data from both provinces line up on the same heat flux-heat production relationship [*Birch et al.*, 1968]. Furthermore, the Appalachians province as a whole lies on a global heat flux-heat production relationship for the major geological provinces of North America, which shows that there is no detectable deep-seated transient heat flux anomaly.

4.2. Calculation Method

[38] To derive vertical profiles of temperature through the lithosphere, we solve the steady-state heat conduction equation in a medium with heat production and temperature-dependent thermal conductivity:

$$\frac{\partial Q}{\partial z} = -A(z), \quad (20)$$

$$\frac{\partial T}{\partial z} = \frac{1}{k(T)}Q(z), \quad (21)$$

where z is depth, T is temperature, Q is the heat flux, A is the heat production, and k is the thermal conductivity. We use temperature-dependent equations for thermal conductivity that are discussed in Appendix C. Boundary conditions at the surface are $Q(z=0) = Q_s$ and $T(z=0) = 0^\circ\text{C}$. We assume that the crust is stratified in two layers, with an upper crust enriched in radiogenic elements with respect to the lower crust. We solve the heat conduction equation down to the depth where geotherms intersect the mantle isentrope. The intersection provides an estimate of the lithospheric thickness. For greater depths, the temperature increases linearly along the isentropic gradient. The equation is solved for parameter values in ranges that are indicated in Table 6 and

Table 6. Input Parameter Values^a

Parameter	Symbol	Value
Thickness of the upper crustal layer	h_1	9.1 km
Total thickness of the crust	h_2	40 km
Average surface heat flux	Q_s	$Q_s^{\text{obs}} \pm \sigma_Q$
Moho heat flux	Q_m	12–18 mW m ⁻²
Heat production in the upper crustal layer	A_{uc}	$\geq 0.35 \mu\text{W m}^{-3}$
Heat production in the lower crustal layer	A_{lc}	$0.35 \mu\text{W m}^{-3}$
Heat production in the lithospheric mantle	A_m	0–0.02 $\mu\text{W m}^{-3}$
Isentropic gradient	γ	$0.5^\circ\text{C km}^{-1}$
Mantle potential temperature	T_{pot}	1250–1450°C

^aHeat production in the upper crust is calculated from the surface heat flux (see equation (23)).

discussed in section 4.3. We generate a large number of geotherms using a Monte Carlo procedure.

[39] The temperature profiles are converted into S wave velocity profiles using the parameterization scheme of *Goes et al.* [2000] and *Shapiro et al.* [2004], which is based on laboratory measurements of thermoelastic properties of mantle minerals and models for the average mineralogical composition of the mantle. We integrate velocity profiles ($v(z)$) to determine the travel time τ through a depth interval extending from 60 to 300 km,

$$\tau = \int_{z_0}^{z_b} \frac{dz}{v(z)} \quad (22)$$

where $z_0 = 60$ km and $z_b = 300$ km. The choice of this depth interval is justified by *Lévy et al.* [2010]. We expect that traveltimes anomalies are restricted to the lithosphere and that no variations exist in the well-mixed convecting mantle. It follows that no traveltimes differences originate deeper than the thickest part of the lithosphere. We require the calculated traveltimes differences between distinct geographical windows to be consistent with those from the NA04 tomographic model. This considerably restricts the parameter ranges.

[40] We first evaluate implications for the mantle potential temperature and derive upper and lower bounds. We then fix the potential temperature to lie within the allowed range and calculate the lithosphere thickness and basal heat flux. From the values of the potential temperature and lithosphere thickness, we determine the maximum heat flux that small-scale convection can supply to the lithosphere. Diffusion and dislocation creep mechanisms are considered, and uncertainties on rheological parameters are taken into account. A comparison between the calculated rheological heat flux and the basal heat flux derived from the data leads to constraints on the deformation mechanism of the sub-lithospheric mantle. Finally, we discuss the implications of our results for the nature of the lithosphere in two provinces (Superior and Appalachians).

4.3. Parameter Values for Temperature Calculations

[41] Parameters involved in the calculation of geotherms are summarized in Table 6. Where crustal thickness estimates are available, they are almost everywhere within a narrow range of 38–45 km [*Perry et al.*, 2002]. Seismic

refraction surveys are not available for many parts of the Canadian Shield, including window I [*Perry et al.*, 2002]. For traveltimes calculations for depths larger than 60 km, however, results are weakly sensitive to changes of Moho depth because of the continuity of heat flux and temperature. We therefore assume a uniform crustal thickness (h_2), which we take to be 40 km. We assume an upper crust of thickness h_1 equal to 9.1 km, as in the work by *Perry et al.* [2006a]. In North America, average values of heat flux and surface heat production for five major provinces of all ages conform to a well-defined linear relationship, which demonstrates that heat production variations in the lower crust are small across the whole continent. This is also supported by geochemical data from both granulite facies terrains [e.g., *Fountain et al.*, 1987; *Shaw et al.*, 1994] and xenolith suites [*Rudnick and Fountain*, 1995]. Exposed granulites yield values of $0.3 \mu\text{W m}^{-3}$, and xenoliths lead to 0.4 – $0.5 \mu\text{W m}^{-3}$. For our model, we fix the lower crustal heat production (A_{lc}) at the mean value of $0.35 \mu\text{W m}^{-3}$.

[42] For each window, the surface heat flux (Q_s) is varied within one standard error of the mean. We allow the Moho heat flux (Q_m) to vary between 12 and 18 mW m⁻². This range is derived from several independent analyses [e.g., *Russell et al.*, 2001; *Mareschal and Jaupart*, 2004; *Perry et al.*, 2006b] and is extensively discussed in Appendix C of *Lévy et al.* [2010]. For each set of values of surface and Moho heat fluxes, heat production in the upper crust (A_{uc}) is readily calculated according to the following equation:

$$A_{uc} = \frac{1}{h_1} (Q_s - Q_m - A_{lc}(h_2 - h_1)). \quad (23)$$

Constraints on heat production in the lithospheric mantle are weak and have been discussed at length by *Rudnick et al.* [1998] and *Michaut et al.* [2007]. We shall allow for variations in the 0 – $0.02 \mu\text{W m}^{-3}$ range.

[43] The well-mixed mantle that lies beneath the continent is characterized by its potential temperature T_{pot} and isentropic gradient γ . The potential temperature refers to the temperature of the isentrope at the atmospheric pressure and is by definition smaller than the temperature at the base of the unstable boundary layer, which is $T_i = T_{\text{pot}} + \gamma H$ (Figure 2). We allow T_{pot} to vary from 1250°C to 1450°C (see section 3.1.1). The value of γ depends on thermodynamic parameters that are known quite accurately [*Navrotsky*, 1995], as well as on the potential temperature. A plausible range extends from 0.3°C to $0.5^\circ\text{C km}^{-1}$ and we shall take a fixed value of $0.5^\circ\text{C km}^{-1}$. Variations of γ within this range are of no consequence for the results of this study, as we only calculate geotherms to a relatively small depth of 300 km. For simplicity, we shall therefore keep the same fixed value of $0.5^\circ\text{C km}^{-1}$ for γ .

5. Potential Temperature of the Mantle Beneath the Canadian Shield

5.1. Range of Acceptable Values

[44] Figures 12 and 13 show the distributions of parameter values for solutions that are consistent with both surface heat flux and traveltimes data. For window K in the Appalachians province, we added a constraint on the upper crustal heat production. We excluded solutions for average

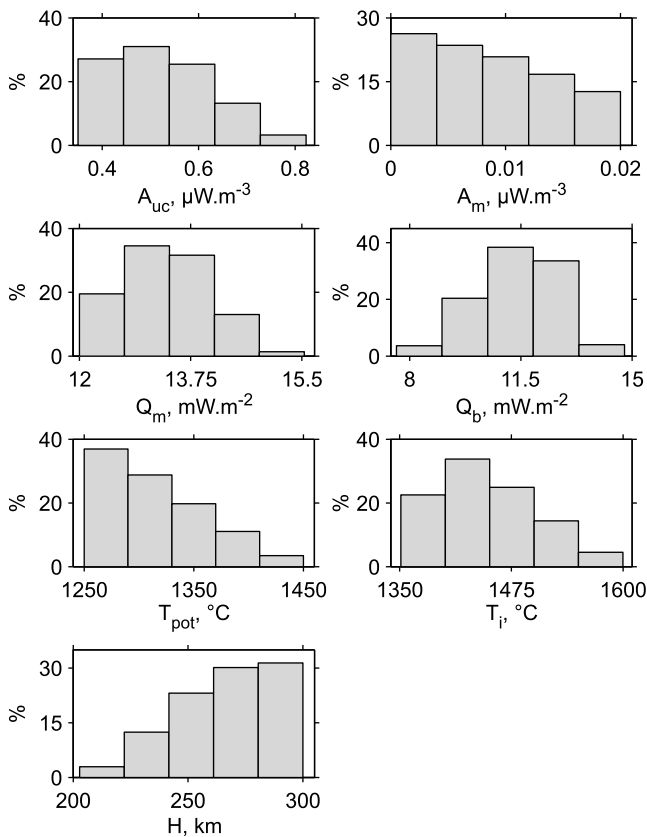


Figure 12. Distribution of parameter values for solutions that are consistent with both surface heat flux and traveltimes for window I. The parameters shown are heat production in the upper crust (A_{uc}) and in the lithospheric mantle (A_m), heat flux at the Moho (Q_m) and at the base of the lithosphere (Q_b), mantle potential temperature (T_{pot}) and temperature at the intersection between the conductive and isentropic profiles (T_i), and lithospheric thickness (H).

values that are larger than $2.8 \mu\text{W m}^{-3}$, because such values are only found locally on enriched plutons and are not representative of the heat production at the scale of the province [Jaupart *et al.*, 1982; Chamberlain and Sonder, 1990].

[45] Window I does not allow us to restrict the range of mantle potential temperatures. However, the results suggest that values larger than 1450°C are unlikely (Figure 12). For window K, no solutions are obtained for temperatures less than 1290°C . Therefore, the mantle potential temperature below North America must be between 1290°C and 1450°C . This range is consistent with that for the oceanic mantle (section 3.1.1 and Table 3), although it has been obtained with completely different methods.

5.2. Relative Contributions of Thermal and Seismic Constraints

[46] Our calculations account for both thermal and seismic constraints. Thermal information comes from heat flux measurements and values of the Moho heat flux taken from previous studies. A detailed review of the Moho heat flux determinations was given by Lévy *et al.* [2010]. The range

of acceptable values that we adopt ($12\text{--}18 \text{ mW m}^{-2}$) is derived from a number of independent constraints, including (P, T) xenolith data [Russell *et al.*, 2001] and surface heat flux and heat production data [Guillou *et al.*, 1994; Mareschal and Jaupart, 2004; Perry *et al.*, 2006b].

[47] To illustrate the relative importance of thermal and seismic constraints, in Figures 14 and 15 we show the distributions of solutions that are obtained for windows I and K when we do not account for traveltimes data. The range for the mantle potential temperature is much larger in this case. In particular, for window K, temperatures as low as 1250°C yield a significant number of solutions. However, the values of heat flux at the surface and at the Moho, on their own, do bring useful constraints on other model parameters, such as the heat flux at the base of the lithosphere, the mantle heat production, and the lithospheric thickness. Thermal and seismic information complement each other and are used simultaneously here.

5.3. Implications and Possible Improvements

[48] The range of acceptable mantle potential temperatures that is obtained is relatively large. Figure 16 illustrates the implications for the lithosphere. Two geotherms were calculated for the two extreme values of the potential temperature and the same parameter values. As the base of the lithosphere is defined by the intersection between the con-

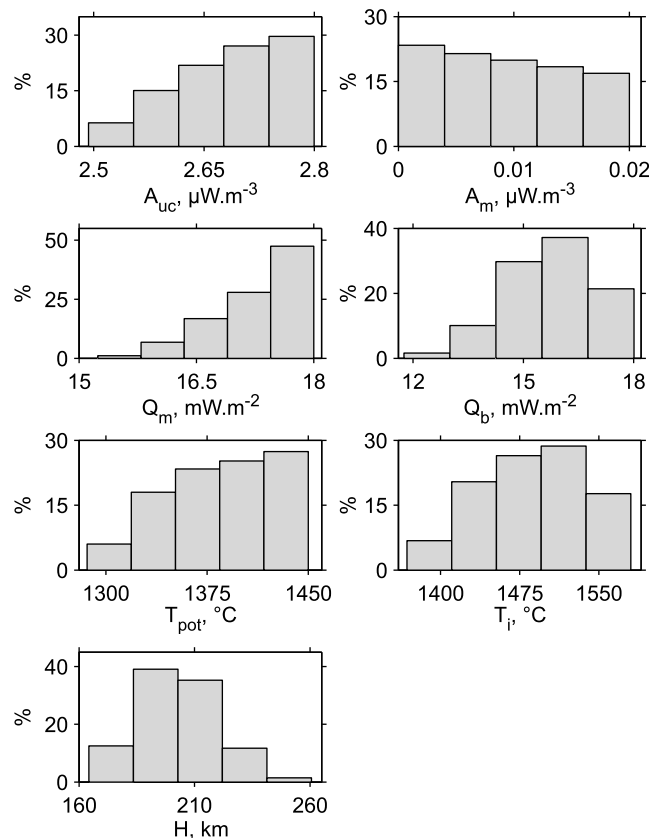


Figure 13. Distribution of parameter values for solutions that are consistent with both surface heat flux and traveltimes for window K. The parameters shown are the same as in Figure 12.

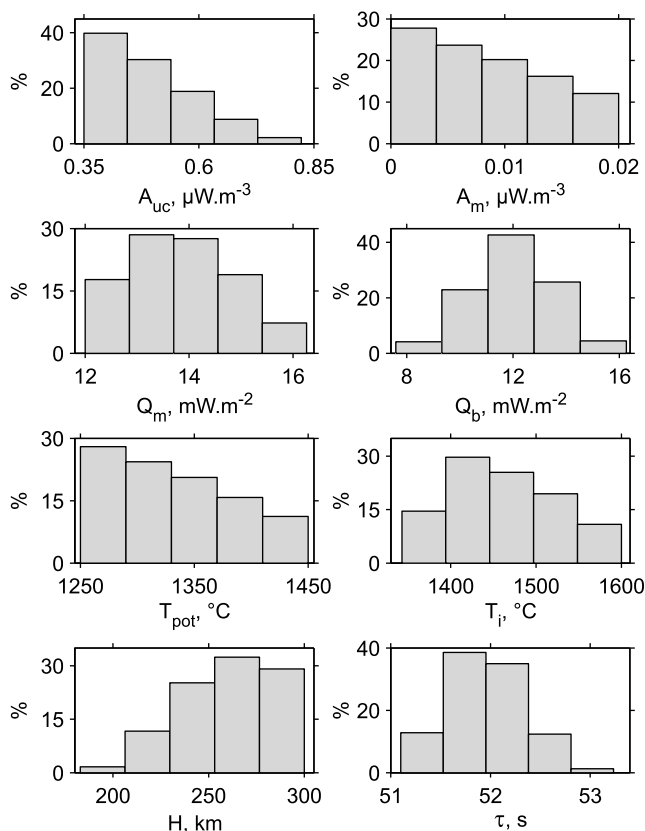


Figure 14. Same as Figure 12 but using constraints from surface heat flux data only for window I. Predicted travel times (over the 60–300 km depth interval) are also represented.

ductive temperature profile and the mantle isentrope, different values of the potential temperature lead to different lithosphere thicknesses. For the parameters used here (see Figure 16 legend), the thickness of the lithosphere is between 217 and 270 km.

[49] Tighter constraints on the mantle potential temperature could be obtained if the other model parameters were known more accurately. The uncertainty on crustal heat production is difficult to estimate. For window K, if enriched plutons are excluded on the grounds that they are isolated anomalies, the upper crustal heat production must be lower than $2.7 \mu\text{W m}^{-3}$. Calculations made with this constraint lead to no significant improvement. One key control variable is heat production in the lithospheric mantle. For instance, if we require it not to exceed $0.01 \mu\text{W m}^{-3}$, the lower bound on the mantle temperature is raised to 1300°C (Figure 17). Conversely, if we impose values that are larger than $0.01 \mu\text{W m}^{-3}$, the upper bound is lowered to 1420°C (Figure 18).

6. Rheology of the Sublithospheric Mantle and Lithospheric Structure

[50] We now investigate implications of the heat flow data for the rheology of the sublithospheric mantle. We focus on small-scale convection. As explained in section 2.1, heating by mantle plumes is unlikely. Heat can also be brought to the lithosphere by underlying mantle that gets swept past it

[Lenardic, 1997; Lenardic and Moresi, 2001; Grigné et al., 2007]. In this case, both the magnitude and lateral variation of the basal heat flux depend on the shape and depth of the lithospheric root, but the key question is whether small-scale convection gets suppressed by large-scale shear. This cannot be answered a priori with the required level of generality if the thickness and temperature difference across the unstable boundary layer that lies beneath the lithosphere are not known. We therefore seek to determine such characteristics and use scalings for small-scale convection.

6.1. Methods

[51] The lithosphere owes its physical properties to partial melting and melt extraction processes which leave a solid residue that is both less dense and mechanically stronger than the starting mantle material. Mechanical strength is due to both temperature, which is lower in the lithosphere than in the underlying convective mantle, and dehydration that occurs during partial melting [Pollack, 1986; Hirth and Kohlstedt, 1996]. One may envision two different controls on the stable lithosphere, which is defined in opposition to the thin unstable thermal boundary layer that lies beneath it. The lithosphere may be identical to the chemically depleted layer, such that stability is due to both buoyancy and enhanced viscosity [Jordan, 1975; Pollack, 1986; Sleep, 2003a]. Alternatively, it may be thicker than the chemically depleted layer and may include a sublayer made of oceanic-type mantle that is too cold and viscous to become unstable [Sleep and Jellinek, 2008]. In the latter case, the

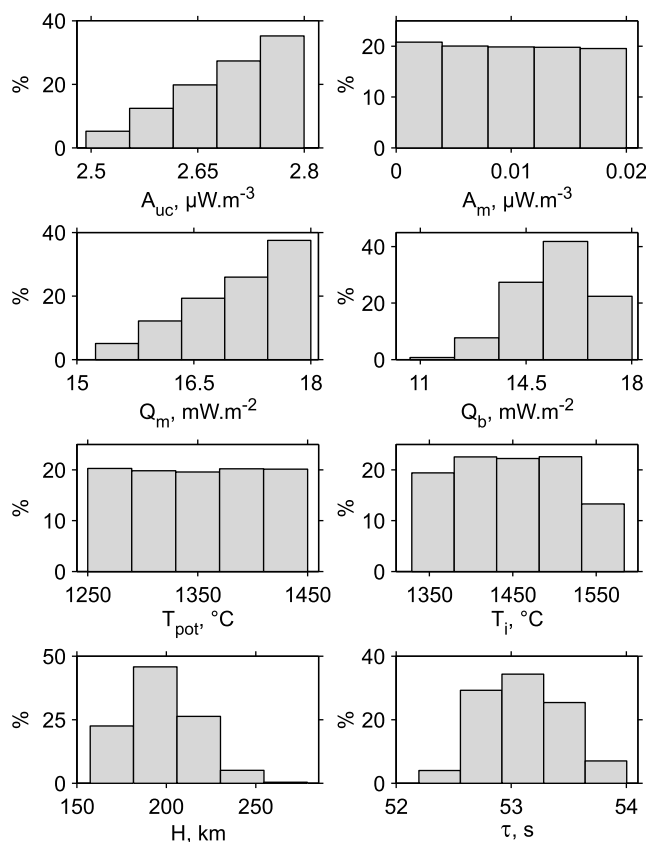


Figure 15. Same as Figure 14 but for window K.

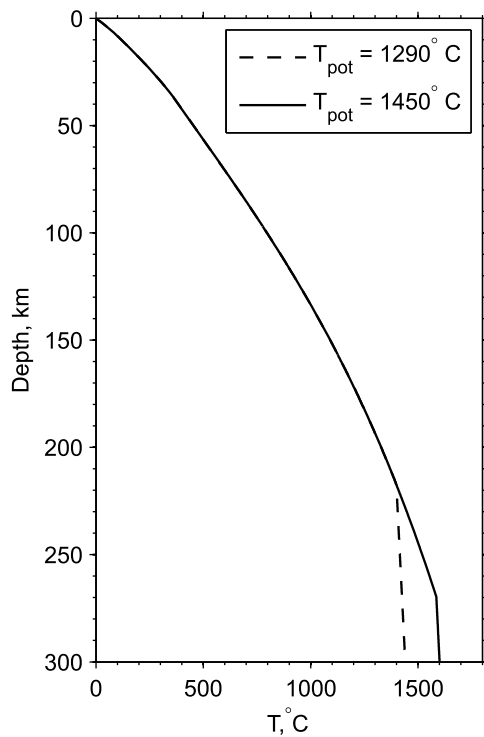


Figure 16. Geotherms for the lowest and highest potential temperatures allowed by our analysis. $Q_s = 40 \text{ mW m}^{-2}$, $Q_m = 15 \text{ mW m}^{-2}$, $A_m = 0.01 \mu\text{W m}^{-3}$, and values indicated in Table 6 for the other parameters. The thickness of the lithosphere differs by more than 50 km for the two geotherms.

unstable boundary layer is dictated solely by the rheological parameters and specifically by the scaling laws described in section 3.1.2. In the former case, the unstable boundary layer may in fact be thinner than the purely rheological one, such that the temperature difference, and hence the heat flux, is smaller than the rheological one. Equations (4) and (8) give the scalings for the rheological heat flux due to diffusion and dislocation creep, respectively.

[52] We first estimate the basal heat flux for the Superior and Appalachians (windows I and K, respectively) using the same method as described in section 4.2. We do not seek constraints on the mantle potential temperature and restrict input values to a narrower range. We consider separately ranges of 1300°C – 1350°C and 1400°C – 1450°C . The other parameters can be found in section 4.3 and Table 6. Figures 19 and 20 show the solution space that is consistent with both heat flux and seismic data for a potential temperature in the 1300°C – 1350°C range. The Superior Province (window I) is characterized by thicker lithosphere and lower basal heat flux than the Appalachians (window K). For window I, the mean thickness of the lithosphere (H_1) is 290 km and the mean basal heat flux (Q_{b1}) is 10.5 mW m^{-2} . For window K, we obtain a mean thickness (H_2) of 183 km and a mean basal heat flux (Q_{b2}) of 16.6 mW m^{-2} . Table 7 lists these results as well as others which have been obtained for larger mantle temperatures.

[53] We use these results to calculate the rheological heat flux values for small-scale convection. We mainly work

with the average basal heat flux and lithospheric thickness, but the validity of our conclusions is also assessed for the end member couples in (H , Q_b) space. The latter are shown in Figure 21 for the temperature range 1300°C – 1350°C . We shall also use the ratio of heat fluxes of windows I and K, which depends only on E , V , and n and not on the pre-exponential proportionality constants in the rheological laws. Using equations (8) and (9), we obtain

$$\frac{Q_1}{Q_2} = \left[\frac{T_1^2(E + P_2V)}{T_2^2(E + P_1V)} \right]^{\frac{2(n+1)}{n+2}} \left[\exp\left(\frac{E + P_2V}{RT_2} - \frac{E + P_1V}{RT_1} \right) \right]^{\frac{1}{n+2}}, \quad (24)$$

where subscripts 1 and 2 refer to the two geographical windows. Finally, we shall discuss the sublithospheric mantle viscosity and compare calculated values with the ones derived from postglacial rebound. Diffusion creep is a Newtonian process, and viscosity is given by equation (1). For dislocation creep, as discussed above, the apparent viscosity is calculated for the small-scale convective flow (equation (10)).

6.2. Results

6.2.1. Overview

[54] The parameters involved in the flow laws that seem to be most uncertain are the activation energy and volume.

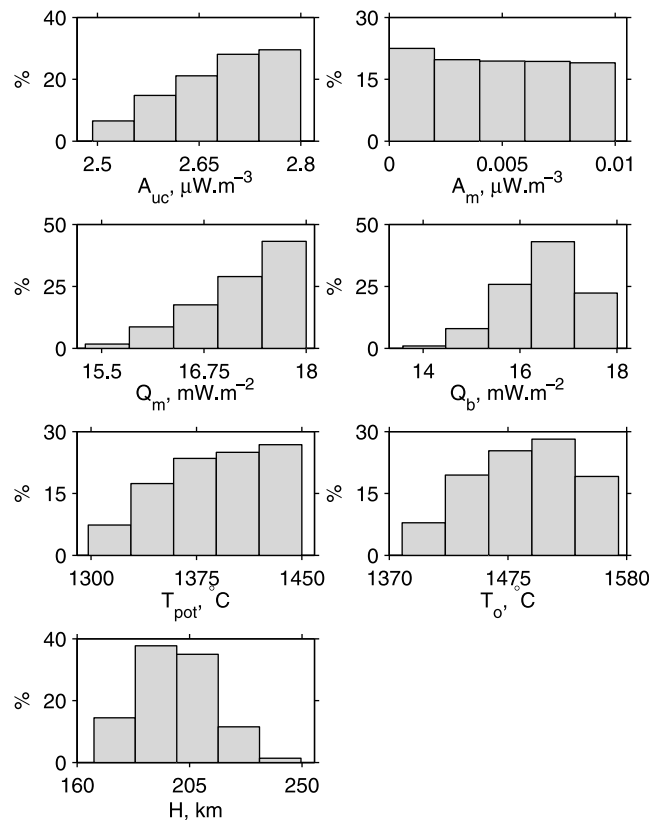


Figure 17. Distribution of parameter values for solutions that are consistent with both surface heat flux and travelttime data for window K for a mantle heat production lower than $0.01 \mu\text{W m}^{-3}$. The parameters shown are the same as in Figure 12.

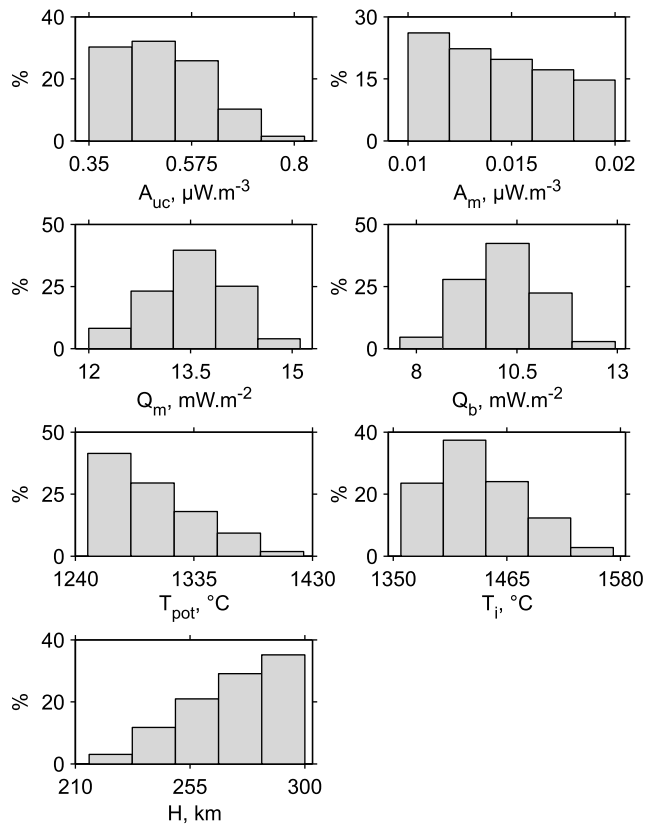


Figure 18. Distribution of parameter values for solutions that are consistent with both surface heat flux and traveltimes for window I for a mantle heat production in the range $0.01\text{--}0.02 \mu\text{W m}^{-3}$. The parameters shown are the same as in Figure 12.

We therefore calculate the range of rheological heat flux values for each deformation mechanism as a function of the activation energy and volume. For wet mantle, we first fix the water content at 800 ppm H/Si [Hirth and Kohlstedt, 1996], following Korenaga and Karato [2008]. Results are shown in Figures 22 and 23. Figures 22 and 23 also indicate the basal heat fluxes determined from the data.

[55] The first striking observation, already outlined in section 3.1.2, is that, with current uncertainties, flow laws cannot be used to predict the basal heat flux. For instance, for wet dislocation creep, which is considered to be the most relevant mechanism in the upper mantle, a range of 7 to 351 mW m^{-2} is allowed for the mantle beneath window I. This emphasizes the necessity to add other constraints.

[56] From Figures 22 and 23, we also can derive new information on the mantle deformation mechanism. Wet diffusion creep does not allow heat fluxes that are large enough. Dry diffusion and dry dislocation creep succeed in explaining the basal heat fluxes of the Superior and the Appalachians, but only for values of the activation energy and volume that are at the lower ends of their respective ranges. Wet dislocation creep clearly allows acceptable values of the basal heat flux and hence is the most likely mantle deformation mechanism, in agreement with Korenaga and Karato [2008].

[57] To account for the values of the basal heat flux for both windows I and K with the same activation energy and

volume, we cannot appeal to the rheological heat flux for both. The flux is either smaller than the rheological one for both, or it is only equal to the rheological one for window K. This is true for wet dislocation creep, but also for the few solutions for dry diffusion and dry dislocation. This has implications for the nature of the lithosphere that are discussed in section 6.3.3.

[58] Finally, it is worth noting that viscosity values corresponding to the acceptable solutions are consistent with those derived from postglacial rebound studies. The latter estimates are derived from a Newtonian model, and hence can only be compared to results for diffusion creep. The viscosity for diffusion creep (equation (1)) does not depend on the temperature difference across the boundary layer and therefore does not depend on whether the temperature difference driving small-scale convection is at its rheological threshold. Solutions for dry diffusion creep yield viscosities between $1.0 \cdot 10^{20}$ and $1.2 \cdot 10^{20} \text{ Pa s}$, close to the range of postglacial rebound estimates, $2.0 \cdot 10^{20}\text{--}5.3 \cdot 10^{20} \text{ Pa s}$ [Cianetti et al., 2002; Mitrovica and Forte, 2004; Paulson et al., 2007]. Just below the lithosphere, viscosity should be slightly lower than such average values (see, e.g., the radial viscosity profile shown by Mitrovica and Forte [2004]), which is in agreement with our results. Viscosities calculated for dislocation creep are similar. For dislocation creep, however, viscosity depends on the temperature difference

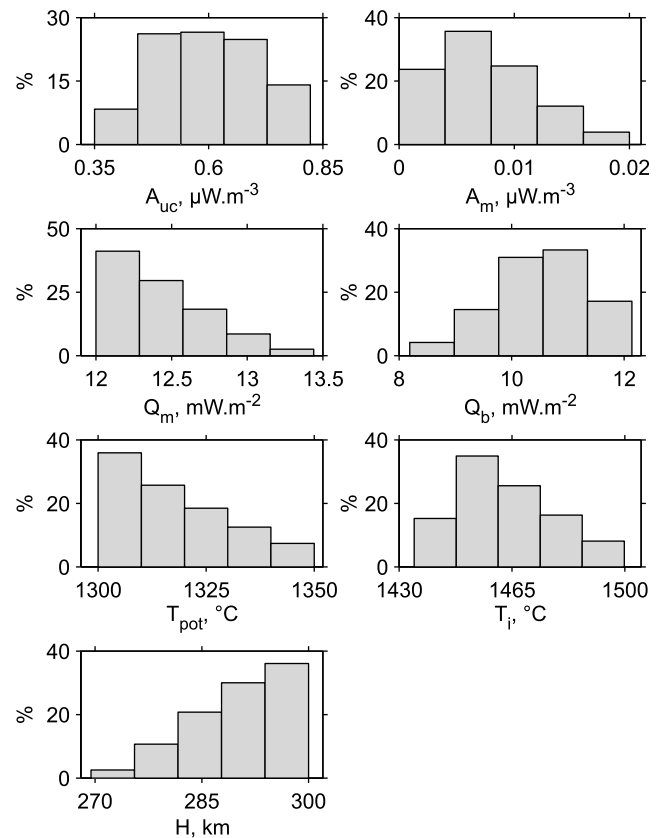


Figure 19. Distribution of parameter values for solutions that are consistent with both surface heat flux and traveltimes for window I for a potential temperature in the $1300\text{--}1350^\circ\text{C}$ range. The parameters shown are the same as in Figure 12.

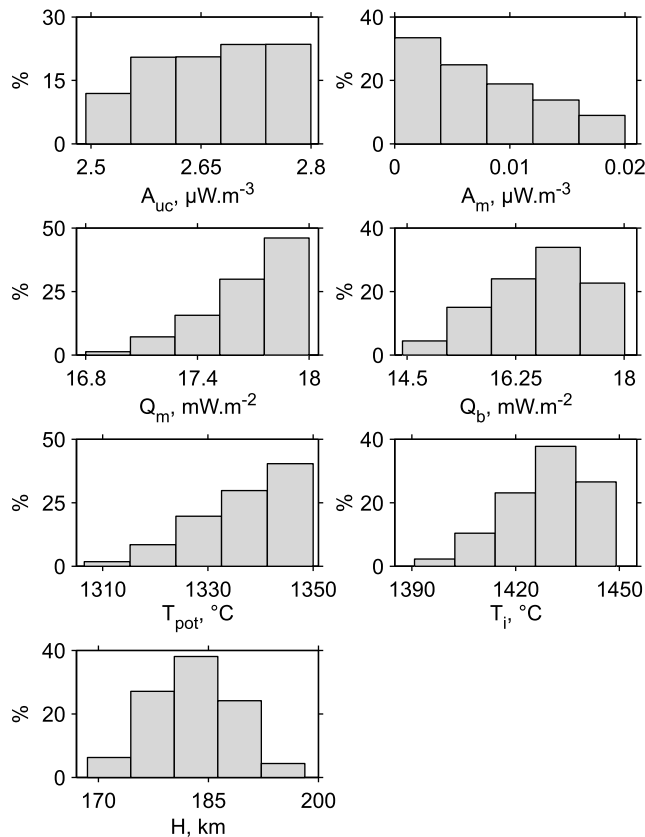


Figure 20. Distribution of parameter values for solutions that are consistent with both surface heat flux and traveltime delays for window K for a potential temperature in a 1300–1350°C range. The parameters shown are the same as in Figure 12.

across the boundary layer. Therefore, in Figure 23, only the value of the viscosity associated with the rheological heat flux for window K should be considered; it is of $1.0 \cdot 10^{20}$ Pa s for wet dislocation. For all the other solutions, observed values for the basal heat flux are smaller than the rheological values, so that the temperature difference driving convection is smaller than the rheological values. In this case, the lithosphere coincides with the chemically depleted layer, and there is no sublayer of stable, undepleted mantle below it and above the unstable thermal boundary layer. For nonlinear creep, therefore, viscosity must be calculated with the temperature difference yielding the correct (observed) basal heat flux (see section 6.3).

6.2.2. Robustness of Our Results

[59] We test the validity of the solutions for the end member couples in the (H, Q_b) solution space (Figure 21). We also assess the influence of rheological parameters other than E and V , and specifically of viscosity coefficient μ_0 for diffusion creep and exponent n for dislocation creep. Finally, we allow for a range of mantle water content and potential temperature.

6.2.2.1. End-Member Couples of the (H, Q_b) Solution Space

[60] The extreme lithospheric thickness–basal heat flux pairs that are consistent with surface heat flux and seismic data are indicated on the solution space shown by Figure 21

for windows I and K. We have compared the rheological heat flux with the observed basal heat flux for each of these couples. Our conclusions are unchanged for wet diffusion and wet dislocation creep. Dry diffusion and dry dislocation creep can only account for the lowest heat flux beneath window K, corresponding to small values of the activation energy and volume. This confirms the preeminence of wet dislocation creep.

6.2.2.2. Uncertainties on the Parameters of the Rheological Laws

[61] We first test the influence of the uncertainty on the viscosity coefficient (equations (13)–(16)). Even with the lowest viscosity coefficient (A at its maximum and p at its minimum), wet diffusion for a water content of 800 ppm H/Si does not give rheological heat fluxes that are large enough to explain the observed ones. Dry diffusion creep must also be excluded if the viscosity coefficient is at its uppermost value. In this case, the heat flux at the base of window K cannot be supplied by small-scale convection. The range of activation energies and volumes yielding acceptable solutions are only very slightly modified by changing the viscosity coefficient. We note on Figure 23 that the observed heat flux values of windows I and K cannot both be explained by rheological heat fluxes. The observed heat flux ratio is not equal to the rheological ratio independently of the viscosity coefficient.

[62] Our conclusions are unchanged for dislocation creep. Heat fluxes depend on the value of exponent n , but the uncertainty on this parameter is in fact too small to induce significant changes.

6.2.2.3. Water Content of the Mantle

[63] So far, we have adopted a water content of 800 ppm H/Si, following *Korenaga and Karato* [2008] and *Hirth and Kohlstedt* [1996]. Such values were obtained from studies of midocean ridge basalts and hence may not be valid for the mantle beneath continents. *Bell and Rossman* [1992] estimated the amount of water in samples from the continental lithospheric mantle beneath British Columbia and South Africa and found values that can be larger than 175 ppm H_2O by weight, corresponding roughly to 2800 ppm H/Si. These samples have had a complex geological history and are probably not representative of the upper mantle. Given the uncertainty regarding the amount of water in the continental, sublithospheric mantle, we consider a wide range of values, from 100 ppm H/Si to 4000 ppm H/Si. We have shown above that diffusion creep with a water content of 800 ppm H/Si does not allow heat fluxes that are large enough, and lowering the water content will not help. Figure 24a shows that even an amount of water as great as 4000 ppm H/Si does

Table 7. Lithospheric Thickness and Basal Thermal Properties Obtained for Windows I and K Using Surface Heat Flux Measurements and Tomographic Traveltime Delays

	Window I	Window K
	$1300 < T_{pot} < 1350^\circ\text{C}$	
Average lithospheric thickness	$H_1 = 290$ km	$H_2 = 183$ km
Average basal heat flux	$Q_{b1} = 10.5$ mW m $^{-2}$	$Q_{b2} = 16.6$ mW m $^{-2}$
Average basal temperature	$T_1 = 1463^\circ\text{C}$	$T_2 = 1429^\circ\text{C}$
	$1400 < T_{pot} < 1450^\circ\text{C}$	
Average lithospheric thickness	$H_1 = 297$ km	$H_2 = 212$ km
Average basal heat flux	$Q_{b1} = 10.7$ mW m $^{-2}$	$Q_{b2} = 15.6$ mW m $^{-2}$
Average basal temperature	$T_1 = 1554^\circ\text{C}$	$T_2 = 1547^\circ\text{C}$

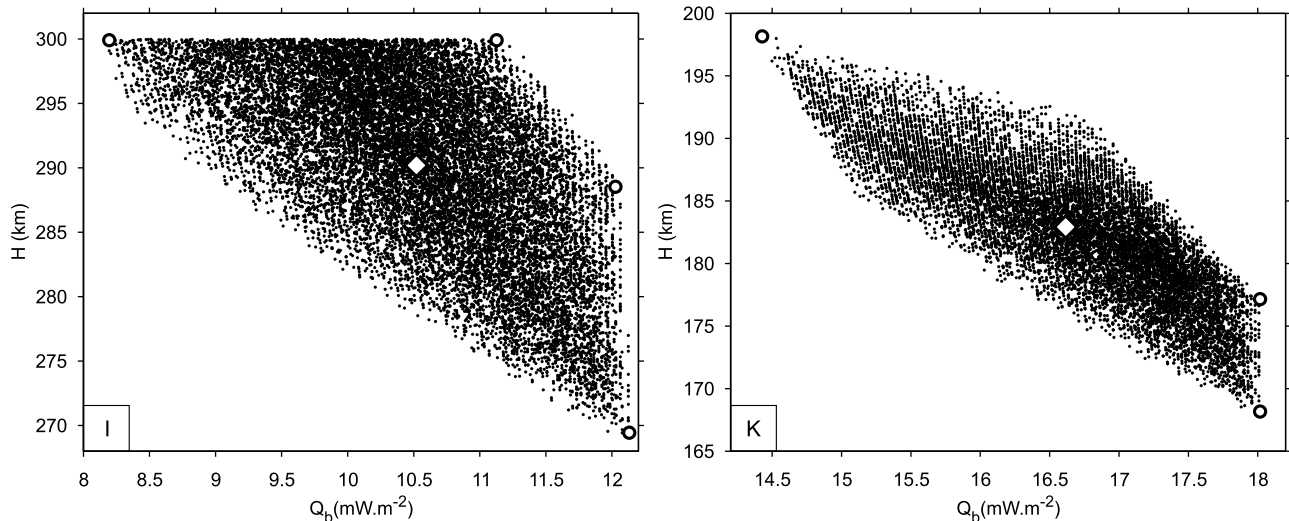


Figure 21. (Q_b, H) solution space for windows (left) I and (right) K for a potential temperature in the 1300–1350°C range. Each dot is a solution. Diamonds mark the average values (Table 7). Circles indicate the end-member solutions.

not sufficiently weaken mantle rocks. For wet dislocation creep, our conclusions are also unchanged whether the water content is 100 ppm H/Si or 4000 ppm H/Si (Figure 24b). Depending on the values of E and V , the observed heat flux can be either lower than the rheological heat flux for both windows I and K or at its rheological value for K. As for the viscosity coefficient, the rheological heat flux ratio does not allow constraints on the water content (equation (24)). Hence, even for amounts of water higher or lower than the range we have considered, the heat flux values would not in any case be at their rheological values for both windows.

6.2.2.4. Influence of the Mantle Potential Temperature

[64] We demonstrate in section 5 that the mantle potential temperature beneath the Canadian Shield is between 1290°C and 1450°C. Existing data do not enable us to reduce this range. However, the potential temperature is unlikely to differ by 160°C between the Superior and Appalachians. As windows I and K are used jointly in this section, we have restricted the mantle potential temperature to a narrower range of 1300°C to 1350°C. Here we proceed to the same calculations, but for a hotter mantle with a potential temperature between 1400°C and 1450°C. The corresponding average lithospheric thicknesses and basal heat fluxes are given in Table 7. Our conclusions are unmodified for diffusion (dry and wet) and for dry dislocation. They are also still valid for wet dislocation. However, in this case, only the very highest values of E and V give a rheological heat flux equal to the basal heat flux of the Appalachians (Figure 25). All other (E, V) couples yield rheological heat flux values larger than the observed one. In this case, the temperature difference across the thermal boundary layer at the base of the lithosphere is thus smaller than the rheological threshold for both provinces.

6.3. Implications

6.3.1. Rheology of the Sublithospheric Mantle

[65] Our results indicate that only the dislocation creep mechanism can meet the heat flux constraints, and furthermore that the mantle must be hydrated. Whatever the water content of the mantle is (within a 100–4000 ppm H/Si range), small-scale convection is able to supply enough heat to the Canadian Shield lithosphere in this deformation regime. Diffusion creep can work, too, but it requires grain sizes of 0.1 mm or less that are not considered realistic [Jackson *et al.*, 2002].

[66] We can characterize the unstable boundary layer at the base of the lithosphere in terms of its temperature difference and effective viscosity. Some sample results are given in Table 8 for various water contents. The temperature difference that drives small-scale convection lies within a rather large range.

6.3.2. Comparison With Data on Mantle Xenoliths

[67] According to Sleep [2003b], the apparent linearity of xenolith (P, T) arrays shows that the temperature difference across the unstable boundary layer beneath continental roots must be smaller than ~300°C. Our solutions are consistent with this bound.

[68] As explained above, the chemical and mechanical lithospheres may not coincide, such that undepleted mantle that is too cold and viscous to become unstable may lie below a chemical layer. Separating the two cannot be done using seismic data alone because of the small influence of composition on seismic velocity [Goes *et al.*, 2000]. Kelly *et al.* [2003] calculated equilibration pressure, temperature, and density for a suite of xenoliths from the Kaapvaal craton and found that they were made of depleted mantle down to depths of at least 200 km. This indicates that the chemical

Figure 22. Heat flux and viscosity for windows (left) I and (right) K as a function of the activation energy E and the activation volume V for diffusion creep. Color scales and isocontours give the rheological heat flux values and the logarithm of the viscosity. Thick lines indicate the values of E and V for which the rheological heat flux equals the observed one.

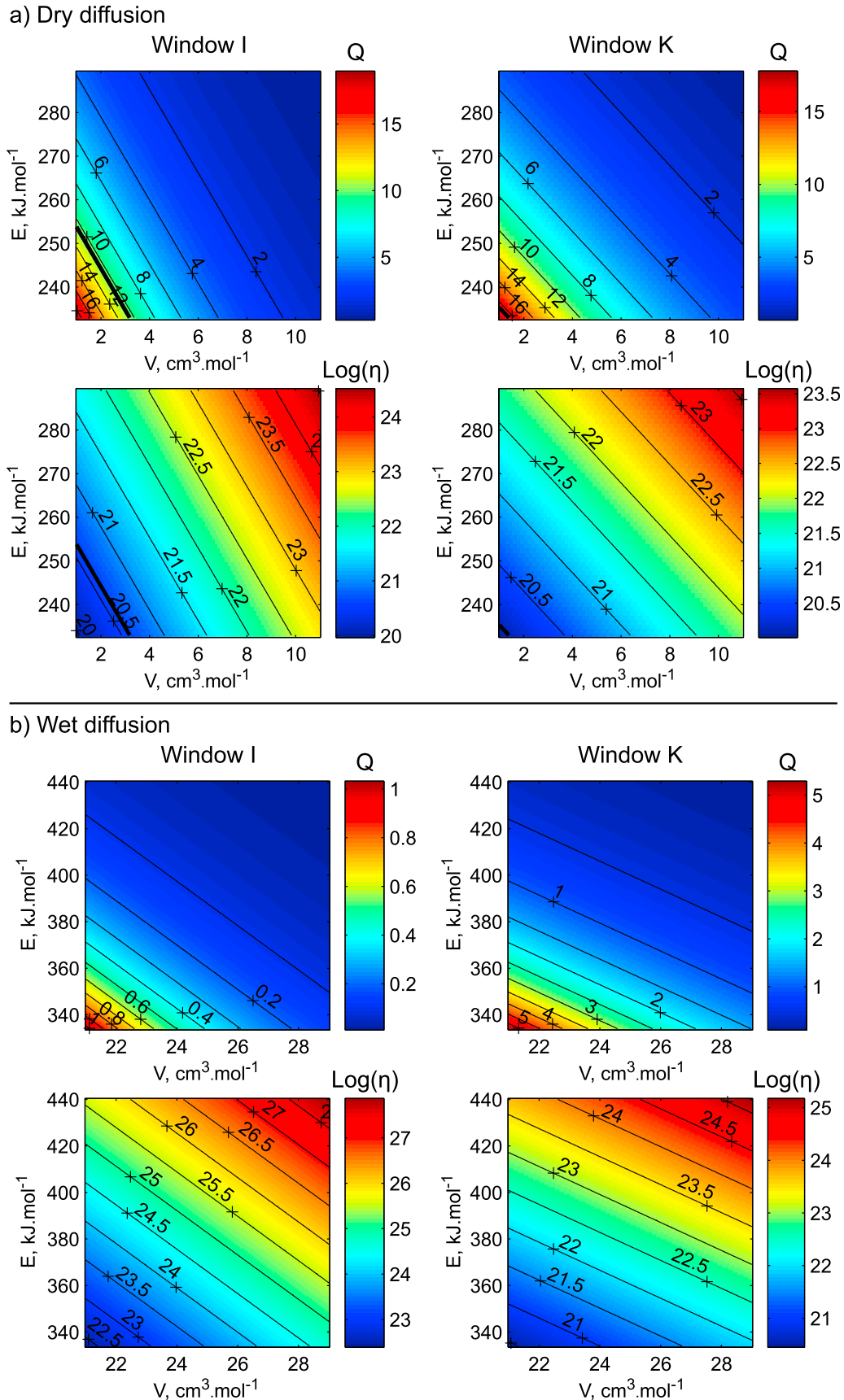


Figure 22

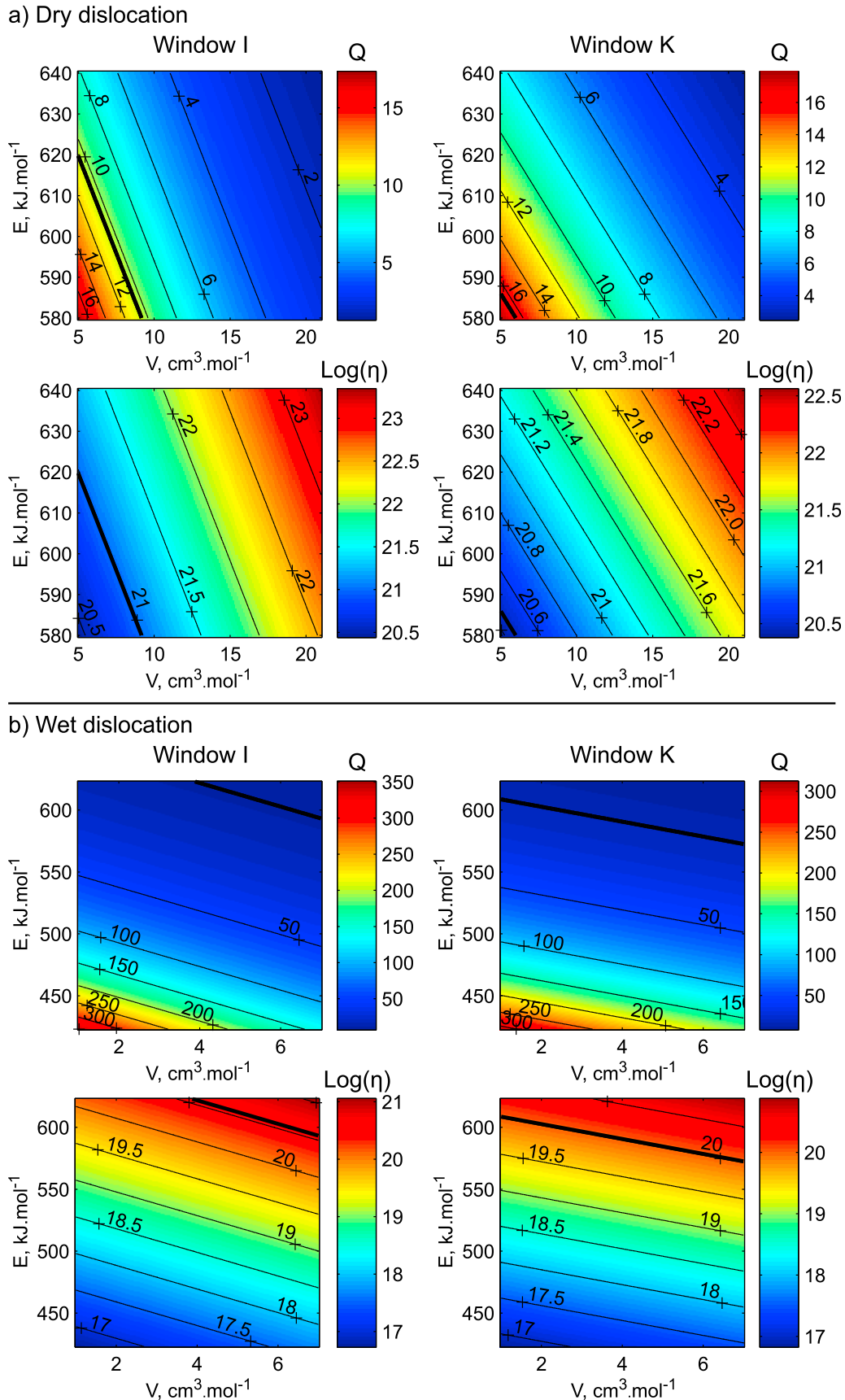


Figure 23

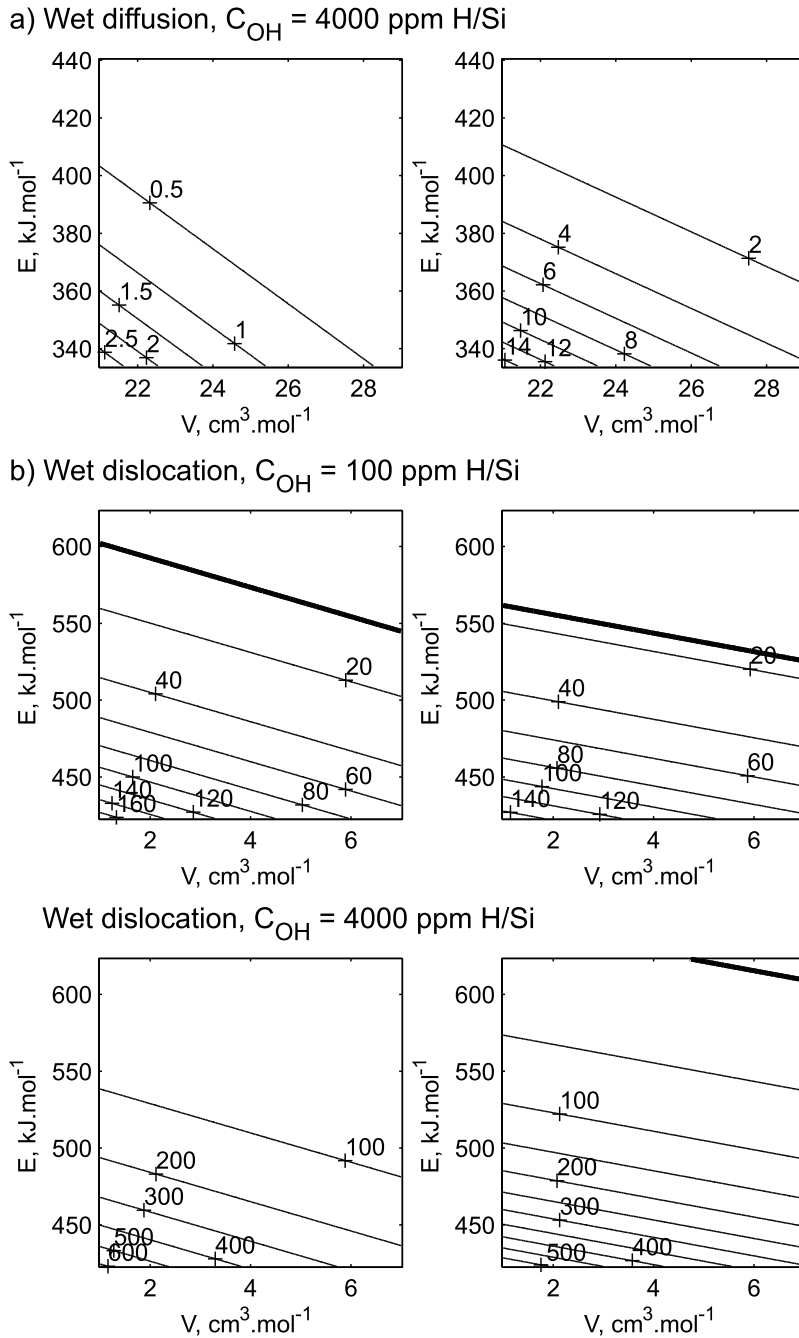


Figure 24. Same as Figures 22b and 23b but for different water contents. Only heat flux diagrams are shown for (left) window I and (right) window K. Even with high water content, wet diffusion creep fails to provide the heat fluxes recorded at the base of the Canadian Shield. On the contrary, wet dislocation creep can explain the basal heat flux values, whatever the amount of water is.

lithosphere extends to at least that depth in this craton. Interestingly, temperature at a depth of 200 km in the chemically depleted Kaapvaal root is about 1400°C . The uncertainty regarding this estimate depends on those on

petrological pressure and temperature determinations and is at least $\pm 50^\circ\text{C}$. Clearly, the temperature of the isentrope at that depth cannot be smaller than that of the xenoliths, which defines a lower bound of $1300^\circ\text{C} \pm 50^\circ\text{C}$ for the

Figure 23. Heat flux and viscosity for windows (left) I and (right) K as a function of the activation energy E and the activation volume V for dislocation creep. Color scales and isocontours give the rheological heat flux values and the logarithm of the corresponding viscosities. Thick lines indicate the values of E and V for which the rheological heat flux equals the observed one.

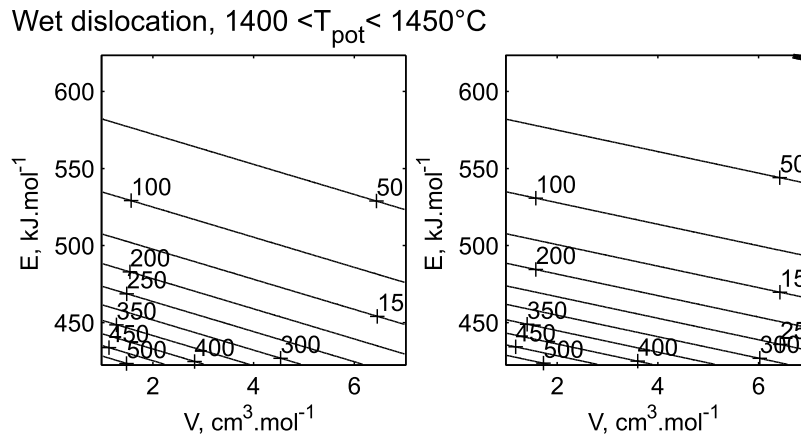


Figure 25. Same as Figure 23b but for a higher potential temperature (in the 1400–1450°C range). Only heat flux diagrams are shown for (left) window I and (right) window K. The basal heat fluxes of both windows are smaller than the rheological ones, except for the highest values of E and V , which allow the observed heat flux of window K to equal the rheological heat flux.

mantle potential temperature. Further, if we take a mantle potential temperature of 1350°C in the middle of the range of acceptable values, the temperature difference across the unstable boundary layer must be 100°C or less. Some of our solutions are consistent with these values (Table 8).

6.3.3. Control of the Lithosphere Thickness

[69] In section 6.2 we show that the basal heat flux that is observed cannot be equal to a rheological value for window I. This implies that there is no stable sublayer of undepleted mantle below the chemically depleted layer in that part of the Superior Province, and hence that the chemical and mechanical lithospheres coincide. This may also be true for the Appalachians, but the large uncertainties regarding the rheological parameters do not allow firm conclusions.

[70] The probable lack of a stable sublayer of cold, undepleted mantle at the base of the chemical lithosphere provides information on how continental roots evolve as they age. Following the extraction of basaltic melts and stabilization in Archean times, continental roots have cooled down because of the decay of its radioactive sources and secular cooling of the whole mantle. Depending on the respective magnitude of these two effects, the temperature difference across the unstable basal boundary layer, ΔT_δ , may have increased or decreased with time. According to Michaut *et al.* [2007], because of the large concentrations of radioelements in continental crust and lithosphere, cooling

due to continental heat sources has probably proceeded faster than secular cooling, so that ΔT_δ has probably increased with time. Thus, if there is no stable, undepleted sublayer below the chemical layer today, there was also none in the past. Thus, the mechanical layer thickness that is observed today is not a recent feature due to the basal accretion of a cold sublayer of upper mantle material.

7. Conclusions

[71] We have combined surface heat flux measurements with a tomographic model to study the structure and properties of both the lithospheric and sublithospheric mantle beneath the Canadian Shield and adjacent provinces. We have found that the potential temperature of the well-mixed convecting mantle lies in a range of 1290°C–1450°C. Constraints on heat production in the lithospheric mantle would tighten this range. The data also indicate that the lithosphere thickness and the basal heat flux both vary laterally by significant amounts across the continent, with a thinner lithosphere and higher basal heat flux values at the eastern edge of the shield beneath the Appalachians.

[72] Assuming that heat is supplied to the continent from below by small-scale convection, we have shown that the most likely deformation mechanism below the lithosphere is dislocation creep in wet mantle. A large range of water

Table 8. Examples of Solutions That Are Consistent With Information Derived From Surface Heat Flux and Tomography for Windows I and K for a Mantle Potential Temperature Between 1300°C and 1350°C^a

	$C_{OH} = 100$ ppm H/Si		$C_{OH} = 800$ ppm H/Si		$C_{OH} = 3000$ ppm H/Si	
	$Q'_b < Q'_{rh}$	$Q'_b = Q'_{rh}$	$Q'_b < Q'_{rh}$	$Q'_b = Q'_{rh}$	$Q'_b < Q'_{rh}$	$Q'_b = Q'_{rh}$
E (kJ mol ⁻¹)	543.6	523.0	590.7	523.0	613.0	523.0
V (cm ³ mol ⁻¹)	4.0	4.0	4.0	4.0	5.3	4.0
Q'_{rh} (mW m ⁻²)	16.5	22.6	16.8	46.7	15.8	74.0
Q'_{rh} (mW m ⁻²)	16.6	22.9	16.6	47.3	16.6	74.9
ΔT_δ (°C)	180.7	154.7	165.7	99.5	162.7	75.2
ΔT_K (°C)	234.0	199.8	216.2	128.6	206.1	97.2
η (Pa s)	2.0×10^{20}	1.1×10^{20}	1.4×10^{20}	1.9×10^{19}	1.3×10^{20}	6.1×10^{18}
η_K (Pa s)	1.4×10^{20}	0.8×10^{20}	1.0×10^{20}	1.3×10^{19}	0.9×10^{20}	4.3×10^{18}

^aThe mantle is assumed to be hydrated and to deform by dislocation creep. Q'_{rh} is a rheological heat flux, Q'_b is the basal heat flux inferred from the data, ΔT_δ is the effective temperature difference across the unstable boundary layer which yields the observed basal heat flux, and η is the corresponding viscosity.

contents (100–4000 ppm H/Si at least) is permissible. Dry diffusion and dislocation creep work only marginally for extremely low activation energies and volumes. Wet diffusion creep is excluded.

[73] We have finally shown that the lithosphere in the Superior province is chemically depleted over its whole thickness. This may also be the case for the Appalachians, but uncertainties in both the data and the rheological parameters do not allow for a firm conclusion.

Appendix A: Seismological Constraints

A1. Seismic Anomalies in the North American Lithosphere

[74] Large-scale coverage in our study area is only provided by surface wave tomography models. We have assessed the robustness of the solutions in different ways [Lévy *et al.*, 2010]. We did not use the full seismic velocity profiles and preferred to use a single datum such as the traveltimes instead, because it is more robust to the inversion procedure, as errors within one depth range are compensated by deviations in other depth ranges. Furthermore, this facilitates comparisons as we are interested in lateral variations of lithospheric structure. We have taken two recent tomographic models: the CUB2.0 global model of Shapiro *et al.* [2004] and the NA04 North American model of van der Lee and Frederiksen [2005]. The CUB2.0 anisotropic model provides Sv and Sh shear wave velocity profiles to a depth of 400 km [Shapiro *et al.*, 2004], whereas the NA04 model provides isotropic values through the whole upper mantle [van der Lee and Frederiksen, 2005]. We also used the totally independent body wave traveltimes data of Wickens and Buchbinder [1980].

[75] We expect that seismic anomalies are largest in the lithosphere and in the underlying thermal boundary layer and that only small variations exist in the well-mixed convecting mantle. It follows that regions that lie below the thickest lithospheric root do not contribute much to traveltimes differences in the upper mantle. Lévy *et al.* [2010] found that traveltimes differences increase with increasing depth range, but that the rate of increase drops markedly below 300 km. In itself, this observation suggests that lithospheric roots do not extend below about 300 km beneath North America. For a total travel time of about 50 s through 250 km thick lithosphere and an uncertainty of ~0.5%, as discussed above, the traveltimes difference of ~0.15 s that is contributed by the 300–400 km horizon is not significant. Larger lateral traveltimes variations are generated by changes of crustal composition and structure. In the study area, the crust can be as thick as 55 km in some regions. For these reasons, we have considered traveltimes anomalies in the 60–300 km depth interval.

[76] The minimum horizontal resolution is about 350 km and 200 km in the horizontal direction in the CUB2.0 and NA04 models, respectively, and about 50 km in the vertical direction in both [Shapiro *et al.*, 2004; Goes and van der Lee, 2002; van der Lee and Frederiksen, 2005]. In the NA04 model, the amplitude of velocity anomalies is well recovered in the upper 250 km and damped at larger depths [Goes and van der Lee, 2002]. Following Shapiro *et al.* [2004], we estimate that the tomographic models have an error of about 0.5% in the lithospheric mantle. The two

surface wave models share many features, with a fast region occupying most of the Canadian Shield that extends to the southeast in a wide corridor. They both indicate that traveltimes variations in North America have an amplitude of 3 s for the depth interval 60–300 km. The overall impression is that the CUB2.0 model is a blurred version of the NA04 one. We previously found [Lévy *et al.*, 2010] that the NA04 model is in remarkable agreement with the body wave data of Wickens and Buchbinder [1980]. We verified that traveltimes delays are poorly sensitive to the size of the averaging window. Lévy *et al.* [2010] concluded that average travel times obtained over the 10 windows of Figure 1b are affected by an uncertainty of ± 0.1 s. We rely on thermal models and are interested in lateral variations of lithospheric structure, so that we only account for the observed traveltimes differences. We consider that a model is acceptable if differences between predicted and observed travel times are less than 0.2 s, which represents a large fraction (10%) of the total variation documented in the study area (Figure 4).

A2. Seismic Travel Time Calculations

[77] To calculate seismic travel times from geotherms, we use the velocity model of Shapiro *et al.* [2004], which accounts for anelastic effects. The many sources of uncertainty have been discussed at length by Shapiro *et al.* [2004] and Lévy *et al.* [2010]. The main ones are the mantle mineralogical composition, the amount of water, and the anelastic correction. In our study, traveltimes anomalies come from the lithospheric mantle, which is believed to be dehydrated [Hirth and Kohlstedt, 1996], so that we have taken water-free parameters. We do account for the presence of water in the convecting mantle. Variations of mineral composition can account for at most 1% difference in seismic velocity in the upper part of the lithosphere and less than this below. On average, the uncertainty over the whole lithosphere is less than ~0.7%, which is comparable to the intrinsic uncertainty regarding traveltimes determinations [Shapiro *et al.*, 2004; Lévy *et al.*, 2010]. A larger uncertainty arises from the anelastic correction, but it is only important at temperatures larger than about 900°C. The magnitude of this correction depends on the physical mechanisms involved as well as on a number of parameters. Shapiro *et al.* [2004] considered two extreme models and obtained a maximum uncertainty of 2% on velocities in the lower part of the lithosphere. Over the whole lithosphere, the implied uncertainty on the travel time is about 1%.

[78] As explained above, we allow for ± 0.1 s uncertainty in traveltimes values. This is not a conservative estimate, but a reasonable one. One of our purposes is to account for both thermal and seismic constraints, and we took care to evaluate separately their respective strengths.

Appendix B: Lithosphere Structure Beneath Eastern North America

[79] Receiver function studies of eastern North America indicate the presence of a relatively shallow (~100 km depth) and sharp interface which has been attributed to the lithosphere-asthenosphere boundary [Rychert *et al.*, 2007]. This interpretation is clearly at odds with heat flow data and has recently been challenged. Three different layers have been identified from changes in the direction of azimuthal anisotropy [Yuan and Romanowicz, 2010]. In the upper

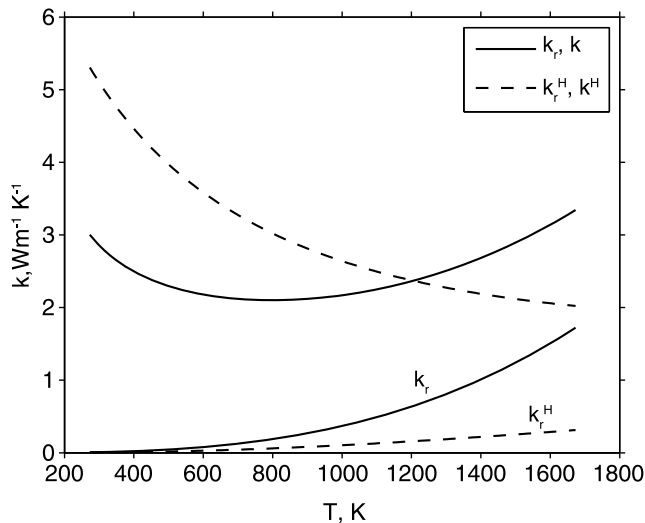


Figure C1. Thermal conductivity as a function of temperature. The solid lines show the temperature dependence used in our study. Dashed lines are from Hofmeister [1999]. Subscript r refers to the radiative contribution.

layer, seismic anisotropy follows the surface geological trends. The base of this layer is deepest beneath the craton and thins toward the edges, and in particular beneath eastern North America, where it coincides with the interface described by Rychert *et al.* [2007]. In the second layer, the anisotropy seems to reflect later accretion of material. The base of this layer is not a sharp interface and lies at a depth of about 200 km beneath the Canadian Shield. It seems to be the true lithosphere-asthenosphere boundary because the direction of anisotropy below is aligned with that of the absolute plate motion.

Appendix C: Thermal Conductivity

[80] Thermal conductivity varies significantly within the range of crustal temperatures. This temperature dependence must be taken into account to calculate accurate geotherms. We adopt the relationship between lattice conductivity and temperature described by Rolandone *et al.* [2002]:

$$k_l(T) = 2.26 - \frac{618.241}{T} + k_o \left(\frac{355.576}{T} - 0.30247 \right), \quad (C1)$$

where T is absolute temperature and k_o is the thermal conductivity at surface conditions ($T = 273$ K), which we take equal to $3 \text{ W m}^{-1}\text{K}^{-1}$. This relationship is derived from measurements on samples from the Superior Province [Durham *et al.*, 1987]. For temperatures higher than 700–800 K, radiative transport becomes important. Laboratory measurements by Schatz and Simmons [1972], Beck *et al.* [1978], and Schärmeli [1979] have led to the following approximate relationship for the radiative contribution:

$$k_r(T) = 0.368 \times 10^{-9} T^3. \quad (C2)$$

In our calculations, conductivity is thus the sum of lattice and radiative components given by equations (C1) and (C2). A detailed discussion of the uncertainty on the radiative

contribution can be found in Appendix B of Lévy *et al.* [2010].

[81] We have evaluated the effects of a different conductivity-temperature relationship on our results. For this purpose, we made some calculations with the conductivity determinations from Hofmeister [1999]. For lattice conductivity, we used the simple expression derived by McKenzie *et al.* [2005] from the results of Hofmeister [1999]:

$$k_l^H(T) = \frac{5.3}{1 + 0.0015(T - 273)}, \quad (C3)$$

where T is absolute temperature. The radiative contribution from Hofmeister [1999] is as follows:

$$k_r^H(T) = 1.753 \times 10^{-2} - 1.0365 \times 10^{-4} T + 2.2451 \times 10^{-7} T^2 - 3.4071 \times 10^{-11} T^3. \quad (C4)$$

These are valid only for the mantle, and hence we have kept the previous expressions for crustal conductivity. As shown in Figure C1, these expressions lead to conductivity values that are significantly lower than those derived from the laboratory measurements of Schatz and Simmons [1972] and Schärmeli [1979].

[82] Figure C2 shows the distribution of solutions obtained using the conductivity values of Hofmeister [1999] for the mantle. The input parameter values are the same as those used for section 5 (Table 6). Comparison of Figure C2 with Figures 12 and 13 shows that results do not change significantly. The potential temperature is less well con-

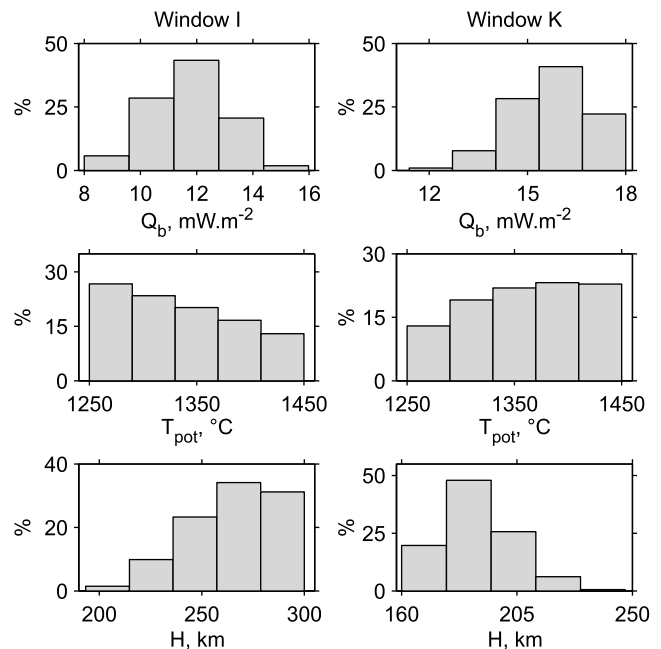


Figure C2. Distribution of solutions obtained using the relationship between conductivity and temperature from Hofmeister [1999]. Solutions are shown for the basal heat flux, potential temperature, and thickness of the lithosphere for windows I (left) and K (right). Input parameters are the same as for Figures 12 and 13 (Table 6). The influence of the conductivity expression on our results is limited.

strained, but solutions for the basal heat flux and thickness of the lithosphere are modified only slightly.

[83] **Acknowledgments.** We thank the Associate Editor, Norman Sleep, and an anonymous reviewer for their useful comments, criticisms, and suggestions which helped us improve the manuscript. Nikolai Shapiro provided his seismic data and functions for the variation of seismic velocity with pressure and temperature.

References

- Bank, C.-G., M. G. Bostock, R. M. Ellis, Z. Hajnal, and J. C. VanDecar (1998), Lithospheric mantle structure beneath the Trans-Hudson Orogen and the origin of diamondiferous kimberlites, *J. Geophys. Res.*, *103*(B5), 10,103–10,114, doi:10.1029/97JB03746.
- Beck, A. E., D. M. Dharba, and H. H. Schloessin (1978), Lattice conductivities of single crystal and polycrystalline materials at mantle pressures and temperatures, *Phys. Earth Planet. Inter.*, *17*, 35–53, doi:10.1016/0031-9201(78)90008-0.
- Bell, D. R., and G. R. Rossman (1992), Water in Earth's mantle: The role of nominally anhydrous minerals, *Science*, *255*, 1391–1397, doi:10.1126/science.255.5050.1391.
- Birch, F., R. F. Roy, and E. Decker (1968), Heat flow and thermal history in New England and New York, in *Studies of Appalachian Geology: Northern and Maritime*, edited by E. Zen et al., pp. 437–451, Interscience, New York.
- Chamberlain, C. P., and L. J. Sonder (1990), Heat-producing elements and the thermal and baric patterns of metamorphic belts, *Science*, *250*, 763–769, doi:10.1126/science.250.4982.763.
- Cianetti, S., C. Giunchi, and G. Spada (2002), Mantle viscosity beneath the Hudson Bay: An inversion based on the Metropolis algorithm, *J. Geophys. Res.*, *107*(B12), 2352, doi:10.1029/2001JB000585.
- Davaille, A., and C. Jaupart (1993), Transient high-Rayleigh-number thermal convection with large viscosity variations, *J. Fluid Mech.*, *253*, 141–166, doi:10.1017/S0022112093001740.
- Doin, M.-P., L. Fleitout, and U. Christensen (1997), Mantle convection and stability of depleted and undepleted continental lithosphere, *J. Geophys. Res.*, *102*, 2771–2787, doi:10.1029/96JB03271.
- Durham, W. B., V. V. Mirkovich, and H. C. Heard (1987), Thermal diffusivity of igneous rocks at elevated pressure and temperature, *J. Geophys. Res.*, *92*, 11,615–11,634, doi:10.1029/JB092iB11p11615.
- Forte, A. M., R. Moucha, N. A. Simmons, S. P. Grand, and J. X. Mitrova (2010), Deep-mantle contributions to the surface dynamics of the North American continent, *Tectonophysics*, *481*, 3–15, doi:10.1016/j.tecto.2009.06.010.
- Fouch, M. J., D. E. James, J. C. VanDecar, and S. van der Lee (2004), Mantle seismic structure beneath the Kaapvaal and Zimbabwe cratons, *S. Afr. J. Geol.*, *107*(1–2), 33–44, doi:10.2113/107.1-2.33.
- Fountain, D. M., M. H. Salisbur, and K. P. Furlong (1987), Heat production and thermal conductivity of rocks from the Pikwitonei-Sachigo continental cross-section, central Manitoba: Implications for the thermal structure of Archean crust, *Can. J. Earth Sci.*, *24*, 1583–1594.
- Goes, S., and S. van der Lee (2002), Thermal structure of the North American uppermost mantle inferred from seismic tomography, *J. Geophys. Res.*, *107*(B3), 2050, doi:10.1029/2000JB000049.
- Goes, S., R. Govers, and P. Vacher (2000), Shallow mantle temperatures under Europe from P and S wave tomography, *J. Geophys. Res.*, *105*, 11,153–11,169, doi:10.1029/1999JB900300.
- Grigné, C., S. Labrosse, and P. J. Tackley (2007), Convection under a lid of finite conductivity: Heat flux and application to continents, *J. Geophys. Res.*, *112*, B08402, doi:10.1029/2005JB004192.
- Guillou, L., J.-C. Mareschal, C. Jaupart, C. Gariépy, G. Bienfait, and R. Lapointe (1994), Heat flow, gravity and structure of the Abitibi belt, Superior Province, Canada: Implications for mantle heat flow, *Earth Planet. Sci. Lett.*, *122*, 103–123, doi:10.1016/0012-821X(94)90054-X.
- Hirth, G., and D. L. Kohlstedt (1996), Water in the oceanic upper mantle: Implications for rheology, melt extraction and the evolution of the lithosphere, *Earth Planet. Sci. Lett.*, *144*, 93–108, doi:10.1016/0012-821X(96)00154-9.
- Hofmeister, A. M. (1999), Mantle values of thermal conductivity and the geotherm from phonon lifetimes, *Science*, *283*, 1699–1706, doi:10.1126/science.283.5408.1699.
- Humler, E., and J. Besse (2002), A correlation between mid-ocean-ridge basalt chemistry and distance to continents, *Nature*, *419*, 607–609, doi:10.1038/nature01052.
- Jackson, I., J. D. Fitz Gerald, U. H. Faul, and B. H. Tan (2002), Grain-size-sensitive seismic wave attenuation in polycrystalline olivine, *J. Geophys. Res.*, *107*(B12), 2360, doi:10.1029/2001JB001225.
- Jaupart, C., J. R. Mann, and G. Simmons (1982), A detailed study of the distribution of heat flow and radioactivity in New Hampshire (U.S.A.), *Earth Planet. Sci. Lett.*, *59*, 267–287, doi:10.1016/0012-821X(82)90131-5.
- Jaupart, C., J. C. Mareschal, L. Guillou-Frottier, and A. Davaille (1998), Heat flow and thickness of the lithosphere in the Canadian Shield, *J. Geophys. Res.*, *103*, 15,269–15,286, doi:10.1029/98JB01395.
- Jordan, T. H. (1975), The continental tectosphere, *Rev. Geophys.*, *13*, 1–12, doi:10.1029/RG013i003p00001.
- Jurine, D., C. Jaupart, and G. Brandeis (2005), Penetration of mantle plums through depleted lithosphere, *J. Geophys. Res.*, *110*, B10104, doi:10.1029/2005JB003751.
- Katsura, T., et al. (2004), Olivine-wadsleyite transition in the system (Mg, Fe)₂SiO₄, *J. Geophys. Res.*, *109*, B02209, doi:10.1029/2003JB002438.
- Kelly, R. K., P. B. Kelemen, and M. Jull (2003), Buoyancy of the continental upper mantle, *Geochem. Geophys. Geosyst.*, *4*(2), 1017, doi:10.1029/2002GC000399.
- Kinzler, R. J., and T. L. Grove (1992), Primary magmas of mid-ocean ridge basalts: 2. Applications, *J. Geophys. Res.*, *97*, 6907–6926, doi:10.1029/91JB02841.
- Korenaga, J. (2003), Energetics of mantle convection and the fate of fossil heat, *Geophys. Res. Lett.*, *30*(8), 1437, doi:10.1029/2003GL016982.
- Korenaga, J., and S.-I. Karato (2008), A new analysis of experimental data on olivine rheology, *J. Geophys. Res.*, *113*, B02403, doi:10.1029/2007JB005100.
- Lee, C.-T. A., A. Lenardic, C. M. Cooper, F. Niu, and A. Levander (2005), The role of chemical boundary layers in regulating the thickness of continental and oceanic thermal boundary layers, *Earth Planet. Sci. Lett.*, *230*, 379–395, doi:10.1016/j.epsl.2004.11.019.
- Lee, C.-T. A., P. Luffi, T. Plank, H. Dalton, and W. P. Leeman (2009), Constraints on the depths and temperatures of basaltic magma generation on Earth and other terrestrial planets using new thermobarometers for mafic magmas, *Earth Planet. Sci. Lett.*, *279*, 20–33, doi:10.1016/j.epsl.2008.12.020.
- Lenardic, A. (1997), On the heat flow variation from Archean cratons to Proterozoic mobile belts, *J. Geophys. Res.*, *102*, 709–721, doi:10.1029/96JB02849.
- Lenardic, A., and L. Moresi (2001), Heat flow scaling for mantle convection below a conducting lid: Resolving seemingly inconsistent modeling results regarding continental heat flow, *Geophys. Res. Lett.*, *28*, 1311–1314, doi:10.1029/2000GL008484.
- Lévy, F., C. Jaupart, J. C. Mareschal, G. Bienfait, and A. Limare (2010), Low heat flux and large variations of lithospheric thickness in the Canadian Shield, *J. Geophys. Res.*, *115*, B06404, doi:10.1029/2009JB006470.
- Mareschal, J. C., and C. Jaupart (2004), Variations of surface heat flow and lithospheric thermal structure beneath the North American craton, *Earth Planet. Sci. Lett.*, *223*, 65–77, doi:10.1016/j.epsl.2004.04.002.
- McKenzie, D., and M. J. Bickle (1988), The volume and composition of melt generated by extension of the lithosphere, *J. Petrol.*, *29*, 625–679.
- McKenzie, D., J. Jackson, and K. Priestley (2005), Thermal structure of oceanic and continental lithosphere, *Earth Planet. Sci. Lett.*, *233*, 337–349, doi:10.1016/j.epsl.2005.02.005.
- Michaut, C., C. Jaupart, and D. R. Bell (2007), Transient geotherms in Archean continental lithosphere: New constraints on thickness and heat production of the subcontinental lithospheric mantle, *J. Geophys. Res.*, *112*, B04408, doi:10.1029/2006JB004464.
- Mitrova, J. X., and A. M. Forte (2004), A new inference of mantle viscosity based upon joint inversion of convection and glacial isostatic adjustment data, *Earth Planet. Sci. Lett.*, *225*, 177–189, doi:10.1016/j.epsl.2004.06.005.
- Navrotsky, A. (1995), Thermodynamic properties of minerals, in *Mineral Physics and Crystallography: A Handbook of Physical Constants, AGU Ref. Shelf*, vol. 2, edited by T. J. Ahrens, pp. 18–28, AGU, Washington, D. C.
- Parsons, B., and D. McKenzie (1978), Mantle convection and the thermal structure of the plates, *J. Geophys. Res.*, *83*, 4485–4496, doi:10.1029/JB083iB09p04485.
- Paulson, A., S. Zhong, and J. Wahr (2007), Inference of mantle viscosity from GRACE and relative sea level data, *Geophys. J. Int.*, *171*, 497–508, doi:10.1111/j.1365-246X.2007.03556.x.
- Perry, H. K. C., D. W. S. Eaton, and A. M. Forte (2002), A revised crustal model for Canada based on Lithoprobe results, *Geophys. J. Int.*, *150*, 285–294, doi:10.1046/j.1365-246X.2002.01712.x.
- Perry, H. K. C., C. Jaupart, J.-C. Mareschal, and G. Bienfait (2006a), Crustal heat production in the Superior Province, Canadian Shield, and in North America inferred from heat flow data, *J. Geophys. Res.*, *111*, B04401, doi:10.1029/2005JB003893.

- Perry, H. K. C., C. Jaupart, J.-C. Mareschal, and N. M. Shapiro (2006b), Upper mantle velocity-temperature conversion and composition determined from seismic refraction and heat flow, *J. Geophys. Res.*, *111*, B07301, doi:10.1029/2005JB003921.
- Pinet, C., C. Jaupart, J.-C. Mareschal, C. Gariépy, G. Bienfait, and R. Lapointe (1991), Heat flow and structure of the lithosphere in the eastern Canadian shield, *J. Geophys. Res.*, *96*, 19,941–19,963, doi:10.1029/91JB01020.
- Pollack, H. N. (1986), Cratonization and thermal evolution of the mantle, *Earth Planet. Sci. Lett.*, *80*, 175–182, doi:10.1016/0012-821X(86)90031-2.
- Putirka, K. D., M. Perfit, F. J. Ryerson, and M. G. Jackson (2007), Ambient and excess mantle temperatures, olivine thermometry, and active vs. passive upwelling, *Chem. Geol.*, *241*, 177–206, doi:10.1016/j.chemgeo.2007.01.014.
- Rolandone, F., C. Jaupart, J. C. Mareschal, C. Gariépy, G. Bienfait, C. Carbonne, and R. Lapointe (2002), Surface heat flow, crustal temperatures and mantle heat flow in the Proterozoic Trans-Hudson Orogen, Canadian Shield, *J. Geophys. Res.*, *107*(B12), 2341, doi:10.1029/2001JB000698.
- Rondenay, S., M. G. Bostock, T. Hearn, D. J. White, and R. M. Ellis (2000), Lithospheric assembly and modification of the SE Canadian Shield: Abitibi-Grenville teleseismic experiment, *J. Geophys. Res.*, *105*, 13,735–13,754, doi:10.1029/2000JB900022.
- Roy, S., and R. U. M. Rao (2000), Heat flow in the Indian shield, *J. Geophys. Res.*, *105*, 25,587–25,604, doi:10.1029/2000JB900257.
- Rudnick, R. L., and D. M. Fountain (1995), Nature and composition of the continental crust: A lower crustal perspective, *Rev. Geophys.*, *33*(3), 267–309, doi:10.1029/95RG01302.
- Rudnick, R. L., W. F. McDonough, and R. J. O'Connell (1998), Thermal structure, thickness and composition of continental lithosphere, *Chem. Geol.*, *145*, 395–411, doi:10.1016/S0009-2541(97)00151-4.
- Russell, J. K., G. M. Dipple, and M. G. Kopylova (2001), Heat production and heat flow in the mantle lithosphere, Slave craton, Canada, *Phys. Earth Planet. Inter.*, *123*, 27–44, doi:10.1016/S0031-9201(00)00201-6.
- Rychert, N. H., S. Rondenay, and K. M. Fischer (2007), P-to-S and S-to-P imaging of a sharp lithosphere-asthenosphere boundary beneath eastern North America, *J. Geophys. Res.*, *112*, B08314, doi:10.1029/2006JB004619.
- Schärmeli, G. (1979), Identification of radioactive thermal conductivity in olivine up to 25 kbar and 1500 K, paper presented at 6th AIRAPT Conference, Int. Assoc. for Res. and Adv. of High Pressure Sci. and Technol., Boulder, Colo.
- Schatz, J. F., and G. Simmons (1972), Thermal conductivity of Earth materials at high temperatures, *J. Geophys. Res.*, *77*, 6966–6983, doi:10.1029/JB077i035p06966.
- Shapiro, N. M., M. H. Ritzwoller, J. C. Mareschal, and C. Jaupart (2004), Lithospheric structure of the Canadian Shield inferred from inversion of surface-wave dispersion with thermodynamic a priori constraints, in *Geological Prior Information: Informing Science and Engineering*, edited by A. Curtis and R. Wood, *Geol. Soc. Spec. Publ.*, *239*, 175–194, doi:10.1144/GSL.SP.2004.239.01.12.
- Shaw, D. M., A. P. Dickin, H. Li, R. H. McNutt, H. P. Schwarcz, and M. G. Truscott (1994), Crustal geochemistry in the Wawa-Foleyet region, Ontario, *Can. J. Earth Sci.*, *31*, 1104–1121, doi:10.1139/e94-099.
- Sleep, N. H. (1990), Hotspots and mantle plumes: Some phenomenology, *J. Geophys. Res.*, *95*, 6715–6736, doi:10.1029/JB095iB05p06715.
- Sleep, N. H. (2003a), Survival of Archean cratonic lithosphere, *J. Geophys. Res.*, *108*(B6), 2302, doi:10.1029/2001JB000169.
- Sleep, N. H. (2003b), Geodynamic implications of xenolith geotherms, *Geochem. Geophys. Geosyst.*, *4*(9), 1079, doi:10.1029/2003GC000511.
- Sleep, N. H., and A. M. Jellinek (2008), Scaling relationships for chemical lid convection with applications to cratonic lithosphere, *Geochem. Geophys. Geosyst.*, *9*, Q12025, doi:10.1029/2008GC002042.
- Solomatov, V. S. (1995), Scaling of temperature- and stress-dependent viscosity convection, *Phys. Fluids*, *7*, 266–274, doi:10.1063/1.868624.
- Solomatov, V. S., and L.-N. Moresi (2000), Scaling of time-dependent stagnant lid convection: Application to small-scale convection on Earth and other terrestrial planets, *J. Geophys. Res.*, *105*, 21,795–21,817, doi:10.1029/2000JB900197.
- Spasojevic, S., L. Liu, and M. Gurnis (2009), Adjoint models of mantle convection with seismic, plate motion, and stratigraphic constraints: North America since the Late Cretaceous, *Geochem. Geophys. Geosyst.*, *10*, Q05W02, doi:10.1029/2008GC002345.
- van der Lee, S., and A. Frederiksen (2005), Surface wave tomography applied to the North American upper mantle, in *Seismic Earth: Array Analysis of Broadband Seismograms*, *Geophys. Monogr. Ser.*, vol. 157, edited by A. Levander and G. Nolet, pp. 67–80, AGU, Washington, D. C.
- Wickens, A., and G. Buchbinder (1980), S-wave residuals in Canada, *Bull. Seismol. Soc. Am.*, *70*, 809–822.
- Yuan, H., and B. Romanowicz (2010), Lithospheric layering in the North American craton, *Nature*, *466*, 1063–1068, doi:10.1038/nature09332.

C. Jaupart, Équipe de Dynamique des Fluides Géologiques, Institut de Physique du Globe de Paris, 1 rue Jussieu, F-75238 Paris CEDEX 05, France.

F. Lévy, School of Earth and Environment, University of Leeds, Leeds LS2 9JT, UK. (F.C.M.Levy@leeds.ac.uk)